each was examined by contrast-phase microscopy for identification and assessment of germ cell type and percentage per fraction. Only those fractions containing spermatogonia/spermatocytes, round spermatids, elongated spermatids, cytoplast/ residual bodies in purities of at least 70% were pooled and used to isolate their respective content of RNA.

RT-PCR

Four different germ cell fractions (pachytene spermatocytes, round spermatids, elongated spermatids and residual bodies/cytoplasts) were collected and total RNA was extracted using an RNeasy Mini Kit (Qiagen, Mississauga, ON), according to manufacturer's specifications. A fraction of 2 μg of total RNA was used to synthesize cDNA. RT-PCR reaction was performed using Omniscript RT kit (Qiagen, Mississauga, ON). Same amounts of cDNA were used to amplify ABCA17, the loading control was ß-actin. ABCA17 primers were designed based on mouse ABCA17 cDNA sequence accession number NM_001031621.The ABCA17 forward primer was 5'-CAGAGTGGCTGTGTT CAGGA and the ABCA17 reverse primer was 5'-CCCCAGACACTGCCTATGTT corresponding to bases 993-1012 and 1300-1319, respectively. The predicted amplification size was 427 bp. PCR cycling conditions were 94°C for 3 min followed by 30 cycles of 94°C for 30 sec, 60°C for 30 sec, and 72°C for 30 sec, with a final extension for 5 min at 72°C.

Northern blot analysis

Total RNA was extracted from the testes of mice at postnatal days 5 (n=3), 20 (n=3), and 45 (n=3) and from different germ cell fractions using a RNeasy Mini Kit (Qiagen, Mississauga, ON). RNA blot analysis was carried out using a 32P-labelled DNA fragment, which corresponded to nucleotides 2479 to 3342. The hybridization was done under high-stringency conditions as described previously (Ban et al., 2005). Briefly, total RNA (20 μg) was denatured and electrophoresed in 1% (w/v) agarose gel, blotted on a nylon membrane, and hybridized with the ABCA17 cDNA probe. The membrane was exposed to X-ray film with an intensifying screen at -80°C for 4 days.

Immunoblot analysis

Male CD-1 mice at postnatal days 5 (n=3), 20 (n=3), and 45 (n=3) were anesthetised with sodium pentobarbital. Their testes were removed and placed in Dulbecco's Modified Eagle Medium (Invitrogen Corporation, Burlington, ON) containing a protease inhibitor cocktail (Complete Protease Inhibitor Cocktail Tablets, Roche, Palo Alto, CA) and minced using a razor blade and pelleted. The pelleted tissue was resuspended in 100 μl of 1.0% NP40, 154 mM NaCl, 0.4mM Tris pH 8.0 containing protease inhibitors (Roche). After 30 min incubation, the lysate was centrifuged at 10,000xg, 4°C for 10 min. The protein concentration of the supernatant was determined by BioRad Protein Assay (BioRad, Mississauga, ON). Aliquots containing 20 μg total protein were subjected to SDS-PAGE under reducing conditions and transferred to Hybond-ECL nitrocellulose membranes (Amersham Biosciences, Piscataway, NJ). Detection was achieved using the ECL+ Western Blotting Detection System (Amersham Biosciences, Piscataway, NJ) and Kodak BioMax Light Film (Kodak, Montreal, QC). Lysates from different germ cell fractions were also subjected to SDS-PAGE, transferred to Hybond-ECL nitrocellulose membranes and stained with the ABCA17 antibody as described above.

Spermatozoa cholesterol efflux assays

The caput, corpus and cauda epididymides were isolated from euthanized CD1 mice (n=3). The tissue was chopped using a razor blade and transferred to 5 ml of Krebs Ringer bicarbonate medium buffered with HEPES (KRB-HEPES) and kept at 37°C in a water bath for 10 min. The released spermatozoa were pelleted by centrifugation at 500xg, for 10 min at 25°C. The pellets were resuspended in 2 ml of KRB-HEPES (37°C) at a concentration of 1x107 spermatozoa/ml. Subsequently, 100 μl of the cell suspension was mixed with 100 μl of 50 μg/ml human apoAI (Sigma) (in KRB-HEPES) with either: 1) rabbit IgG plus 0.5% NP40; 2) 0.5% NP40; 3) ABCA17 (10 μg IgG/ml); 4) ABCA17 (10 μg IgG/ml) plus 0.5% NP40; 5) ABCA17 (10 μg IgG/ml) plus ABCG1 (5 μg IgG/ml) plus 0.5% NP40; and incubated at 37°C and 5% CO_2 for 1 h. After 1 h incubation, spermatozoa were pelleted by centrifugation at 500xg for 10 min at 25°C. The supernatant was then transferred to a new tube and the spermatozoal pellet was washed once with KRB and then resuspended in 140 μl of PBS. Aliquots (50 μl) of the spermatozoal suspension and supernatant were analyzed for cholesterol using an Amplex Red Cholesterol Kit (Molecular Probes, Eugene, OR) and a PerkinElmer Life Sciences Microplate Reader (PerkinElmer Instruments, Wellesley, MA). Statistical analysis was performed using the t-test.

Results

ABCA17 localization and expression in mouse testis

Immunoperoxidase staining of adult mouse testis sections fixed in Bouin's and reacted with anti-ABCA17 antibody revealed a weak staining of spermatogonia and early spermatocytes and a moderate staining of the cytoplasm of pachytene spermatocytes (Figs. 1A,B). While ABCA17 was not detected in early spermatids, a reaction was noted in the heads and tails of step 12-16 spermatids (stages XII-VIII of the cycle of the seminiferous epithelium) (Fig. 1A,B). Control sections

incubated with non-immune rabbit IgG were completely devoid of staining (Fig. 1C,D).

Spermatozoa isolated from the caput epididymidis and reacted with anti-ABCA17 antibody revealed ABCA17 expression on the dorsal aspect of the sperm heads and on the midpiece of sperm tails (Fig. 1E). By contrast, no reaction was detected in spermatozoa incubated with non-immune rabbit IgG (Fig. 1F).

Immunofluorescent staining of testicular (Fig. 2A) and epididymal (Fig 2B,C) sections treated with zinc fixative revealed a strong reaction on the heads and tails of late spermatids and spermatozoa. Spermatogonia, and pachytene spermatocytes were unreactive. Control sections incubated with non-immune rabbit IgG were

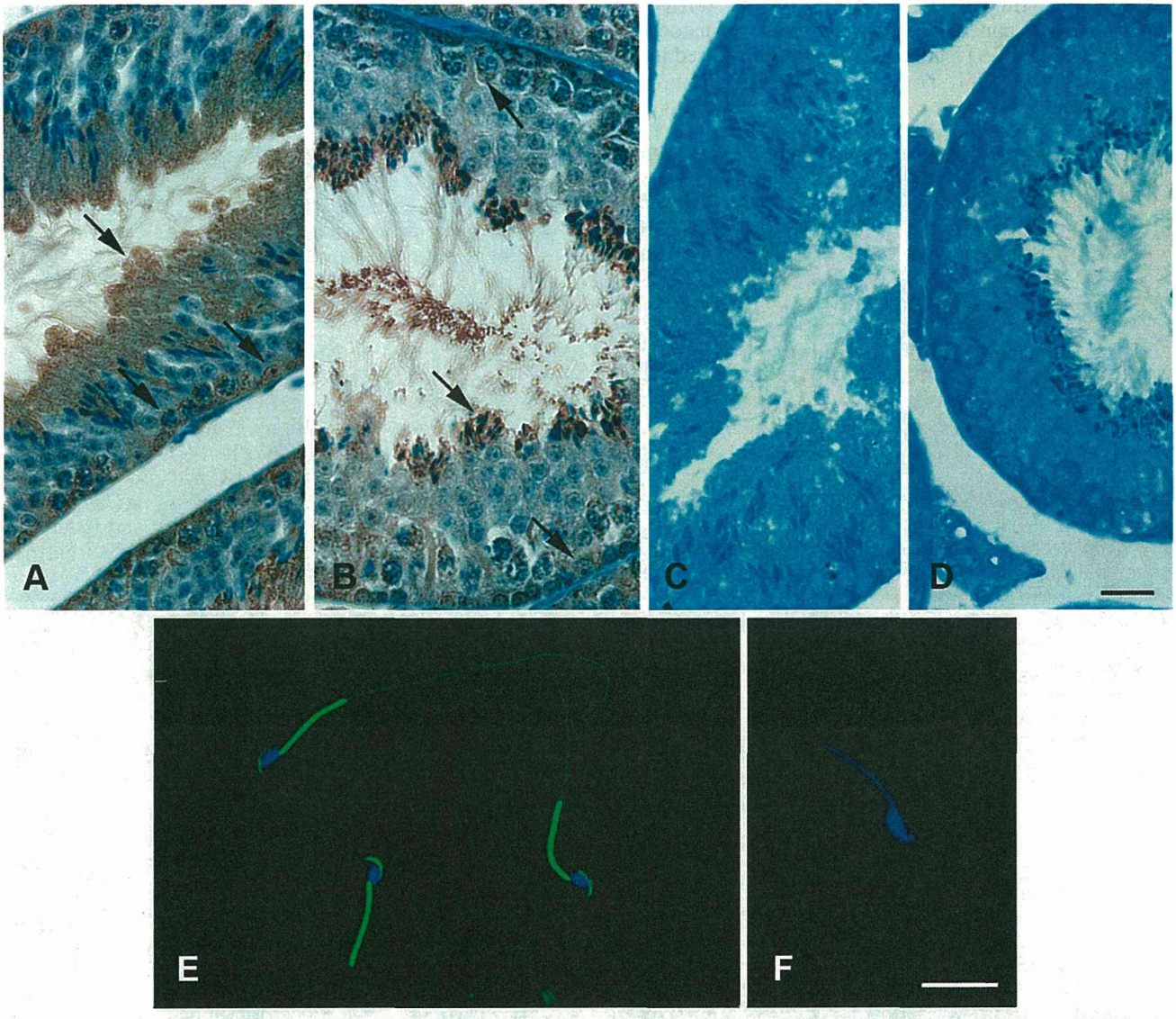

Fig. 1. Immunolocalization of ABCA17 in mouse seminiferous tubules fixed with Bouin's and in spermatozoa isolated from caput epididymidis. **A,** reveals anti-ABCA17 immunoperoxidase staining of a seminiferous tubule at stage II of the cycle. Arrows in **A** point to staining of spermatogonia, pachytene spermatocytes and step 16 spermatids. **B**, shows an immunoperoxidase staining with anti-ABCA17 of a seminiferous tubule at stage VII of the cycle. Arrows in **B** point to staining of spermatogonia, pachytene spermatocytes and step 13 spermatids (located at the luminal border). **C** and **D** are controls IgG immunocytochemical staining of seminiferous tubule at stages II and VII. Bar in panel **D** equals 25 μm and applies to panels **A-C. E,** shows a confocal microscope field of spermatozoa isolated from caput epididymidis immunolabeled with ABCA17 antibody and detected with FITC-conjugated anti-IgG (green). Nuclei were stained with Hoechst 33342 (blue). **F,** is a control IgG staining. Bar in panel **F** equals 10 μm and applies to **E.**

devoid of staining (Fig. 2D).

Developmental expression of ABCA17 in adult mouse testis

ABCA17 transcripts were detected by Northern blot analysis in total testicular RNA isolated from mice at postnatal day 5, 20 and 45. Expression of ABCA17 transcripts (5.3 Kb) in the testis was observed at low levels at day 5, correlating with the appearance of spermatogonia. At postnatal day 20, ABCA17 mRNA expression increased, corresponding with the developmental appearance of pachytene spermatocytes. The level of ABCA17 transcripts further increased in the testis of 45 day old mice, consistent with the presence of both early and elongated spermatids (Fig. 3A).

ABCA17 protein was detected in Western blots of testes at postnatal day 5, 20 and 45. Consistent with findings from Northern blot analysis, relatively low levels of ABCA17 were detected in testicular extracts at postnatal day 5 old mice. However, the level of ABCA17 increased in testis at postnatal day 25 and 45 (Fig. 3B).

Expression of ABCA17 in isolated testicular cells

Spermatogonia, spermatocyte, round spermatids and elongated spermatids were isolated at 70-90% purity by

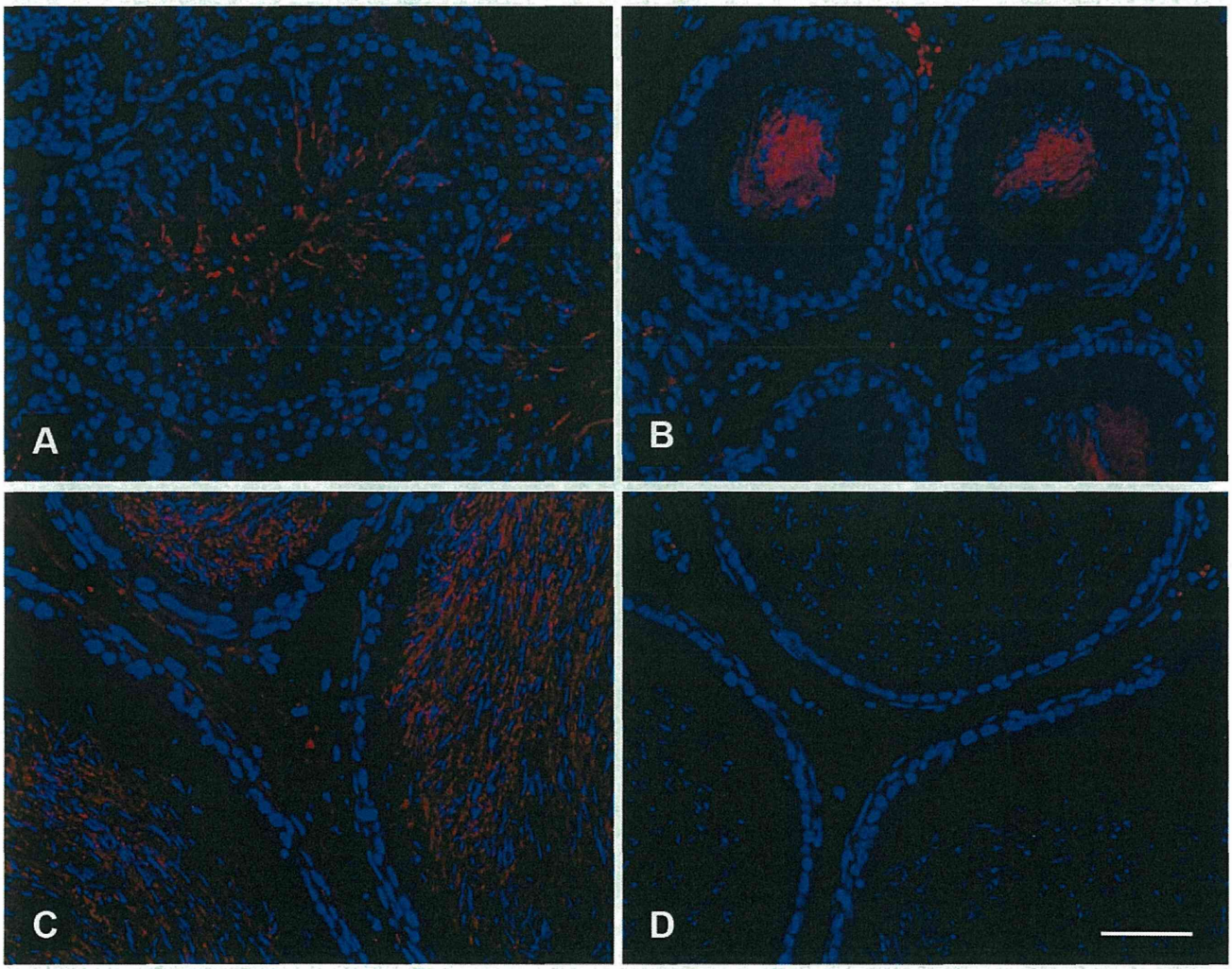

Fig. 2. Immunostaining of ABCA17 in mouse testicular A and epididymal B-D sections preserved with zinc fixative. **A.** ABCA17 antibody reacts specifically with elongated spermatids (stage VI of the cycle). **B, C.** ABCA17 antibody also produces a strong immunofluorescence staining of epididymal luminal spermatozoa (**B**, caput; **C**, cauda). **D**, is a control cauda section incubated with non-immune rabbit IgG. Bar in panel **D** equals 30 μm and applies to all panels.

staput velocity sedimentation on a 1-4% BSA gradient in HBSS. The spermatogonial/spermatocyte fraction (F1; 80% purity) was mainly contaminated with round spermatids. The round spermatid fraction (F2; 90% purity) contained 10% of elongated spermatids. The elongated spermatid fraction (F3; 80% purity) was chiefly contaminated with round spermatids and cytoplasts. The cytoplast/residual bodies/spermatozoal fraction (F4; 90% purity) was contaminated with elongated spermatids. RT-PCR was performed on total RNA isolated from each of the four fractions. The analysis revealed a strong expression of ABCA17 mRNA expression in fraction 1 and 2 and a slight decrease in fraction 3 and 4 (Fig. 4A). Northern blot analysis demonstrated decreasing levels of ABCA17 transcripts in fraction 3 and 4 (Fig. 4B). Immunoblotting of the cell lysates showed low level of expression of ABCA17 in fraction 2 and high levels in fractions 1, 3 and 4. Control ß-actin remained unchanged (Fig. 4C). The plot (Fig. 4D) illustrates the quantitative levels of ABCA17 mRNA and protein relative to ß-actin.

Involvement of specific ABC transporters in spermatozoa cholesterol efflux

Cholesterol efflux analysis was performed on isolated spermatozoa obtained from the caput, corpus and cauda epididymidis incubated in the presence or absence of the anti-ABCA17 antibody (10μg IgG/ml) according to the procedure of Morales et al. (2008). Because the antibody was raised against an internal region of ABCA17, the spermatozoal membrane was permeabilized with a mild treatment of NP40. The ABCA17 antibody in the presence of NP40 produced a 40% inhibition of cholesterol efflux to apoA-1 in spermatozoa isolated from the corpus epididymidis. The inhibition was statistically significant ($p<0.05$) (Fig. 5). This inhibition was further increased when ABCA17 was incubated in the presence of 5 μg IgG/ml of ABCG1. A decrease was also observed in the cauda epididymidis, however, the data was not statistically significant. NP40 alone did not cause any efflux towards the lipid free apoAI. Consistent with the observation that the ABC antibodies reduced cholesterol efflux was the finding that ABC antibody treatment caused an increase in cell-associated cholesterol (7-15% greater) as compared to spermatozoa treated with control IgG (data not shown).

Discussion

Efflux of plasma membrane cholesterol from mammalian sperm occurs during sperm maturation in the epididymis and during capacitation in the uterus and oviduct (Davis, 1981; Visconti et al., 1995). The loss of cholesterol is essential for the sperm acrosome reaction and hyperactivated motility (Davis, 1981; Visconti et al., 1995; Martinez and Morros, 1996; Jones, 1998). In fact, a variety of events leading up to acrosome reaction are mediated by the loss of cholesterol, such as changes in intracellular ion concentrations, increase in intracellular pH, lipid raft migration to the sperm head and initiation of protein phosphorylation-based signaling cascades (Cross and Razy-Faulkner, 1997; Visconti et al., 1999; Shadan et al., 2004).

The efflux of sterols from spermatozoa plasma membranes requires the presence of lipid acceptor molecules (Davis, 1981; Benoff, 1993; Cross, 1998; Travis and Kopf, 2002), and several publications have documented the existence of lipid acceptor molecules such as high-density lipoproteins (HDL) and apolipoproteins AI and J in both the male and female reproductive tracts (Hermo et al., 1991; Sylvester et al., 1991; Jaspard et al., 1996; Martinez and Morros, 1996; Law et al., 1997; Argraves and Morales, 2004). However, an essential step in this process is the presence

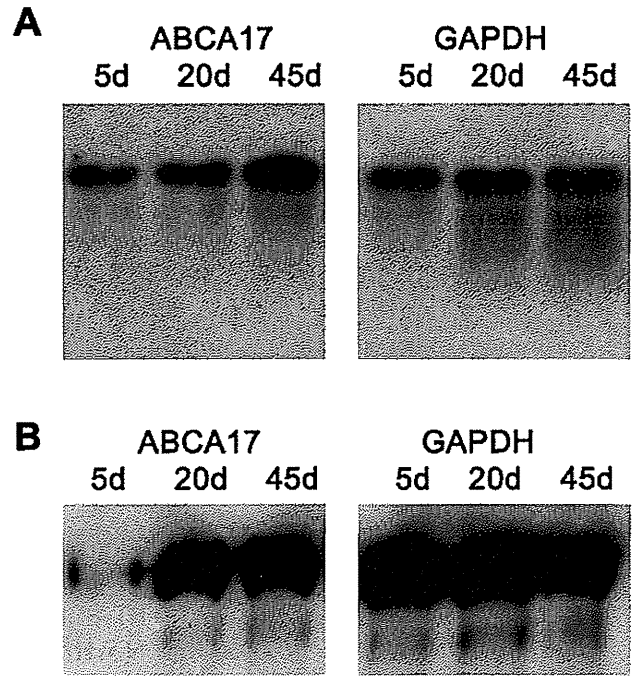

Fig. 3. Developmental expression of ABCA17. **A,** is a Northern blot analysis of testicular RNA and from postnatal 5, 20 and 45 day old mice. The blots are total testicular RNA hybridized with an ABCA17 probe showing low expression of ABCA17 transcripts (5.3 Kb) in testis from postnatal day 5 mice. The level of transcripts increased at postnatal day 20 and 45 (left panel). The right panel is an internal control of the same blot reacted with a GAPDH probe showing unchanged levels of transcripts. B, is an immunoblot of testicular proteins isolated from postnatal 5, 20 and 45 day old mice reacted with anti-ABCA17 antibody (left panel). Low level of ABCA17 was observed at postnatal day 5. The levels of ABCA17 protein increased at postnatal day 25 and 45. The right panel is a control of the same blot reacted with a GAPDH antibody.

of integral proteins capable of transporting sterols from the plasma membrane to the lipid acceptor molecules (Klein et al., 1999). In a past study, our laboratory identified three members of the ATP-binding cassette (ABC) transporter superfamily, ABCA1, ABCA7, and ABCG1 in the sperm plasma membrane (Morales et al., 2008). They were reported to be implicated in the transport of cholesterol to apoAI and albumin. In fact, antibodies to all three of these transporters affected cholesterol efflux from the sperm to lipid acceptors apoAI and albumin and inhibited in vitro fertilization

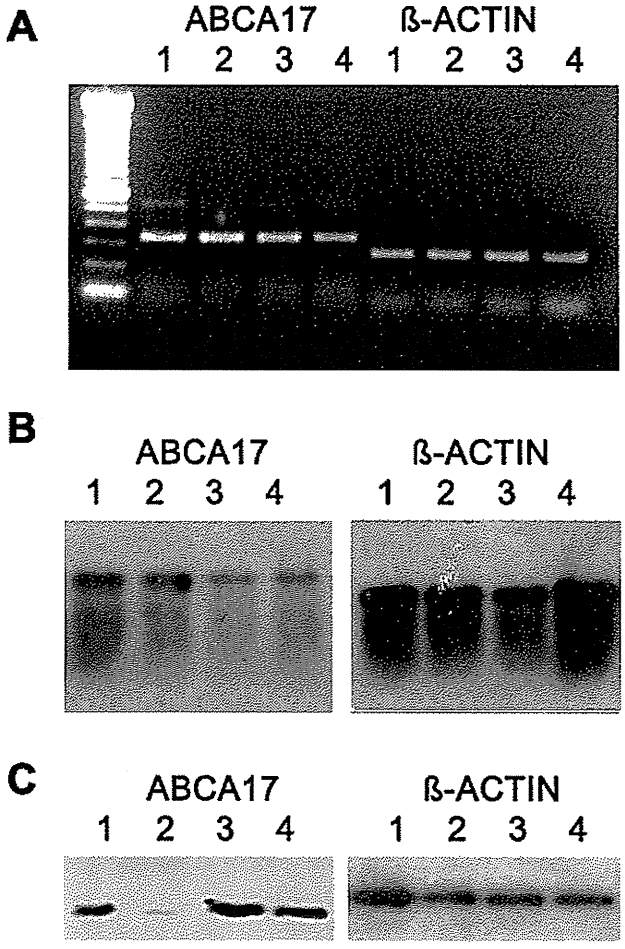

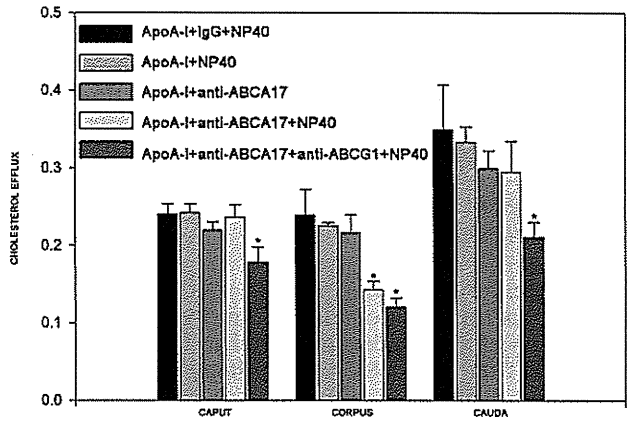

Fig. 5. Effect of ABCA17 antibody treatment on spermatozoa cholesterol efflux. The graph shows levels of spermatozoa cholesterol efflux to apoA-I in the absence or presence of NP40 and antibodies to ABCA17 and ABCG1. In control reactions, spermatozoa were incubated in presence or absence of IgG or NP40. Statistical analysis was performed by t-test. Asterisks indicate that when compared to the three controls the difference is significant ($p<0.05$).

Fig. 4. Expression of ABCA17 in isolated testicular cells. **A**, is a RT-PCR analysis of ABCA17 mRNA expression in adult mouse testis. The RT-PCR was performed in total RNA isolated from germ cells. Fraction 1 (SP) contained spermatogonia and spermatocytes, fraction 2 (RS) round spermatids, fraction 3 (EP) elongated spermatids and cytoplasts, and fraction 4 (RB) cytoplasts, residual bodies and spermatozoa. The analysis revealed a strong expression of ABCA17 mRNA in fractions 1 and 2 and a gradual reduction in fractions 3 and 4 (left panel). Control ß-actin remained unchanged (lanes 1-4, right). **B**, is Northen blot analysis of ABCA17 mRNA expression in adult mouse testis. The blot was performed on total RNA isolated from germ cells as depicted in **A**, revealing high levels of ABCA17 mRNA in fractions 1 and 2 and decreasing levels of ABCA17 transcripts in fractions 3 and 4 (left panel). The right panel is an internal ß-actin control. **C**, is an immunoblot of testicular proteins from isolated germ cells reacted with anti-ABCA17 antibody (left panel). The immunoblot revealed low expression of ABCA17 in fraction 2 and high level of expression in fractions 1, 3 and 4 (left panel). Control ß-actin remained unchanged (right panel). **D**, illustrates the quantitative levels of ABCA17 mRNA (RT-PCR and Northern blot analysis) and protein (immunoblot analysis) relative to ß-actin.

(Morales et al., 2008).

In a recent study, the molecular cloning of the full length cDNA of a novel mouse ATP- binding cassette transporter, ABCA17, which belongs to the A subfamily has been identified (Ban et al., 2005). Metabolic labeling analysis showed that intracellular esterified lipids, including cholesteryl esters were significantly decreased in HEK293 cells stably expressing ABCA17 compared to untransfected cells. Northern blot analysis and quantitative real time PCR revealed that ABCA17 mRNA was expressed exclusively in the testis. While in situ hybridization showed the presence of transcripts in spermatocytes, immunofluorescence with an anti-ABCA17 antibody localized the protein in the anterior head of elongated spermatids and sperm (Ban et al., 2005).

The findings presented herein indicate that ABCA17 transcripts are expressed in all germinal cells. Indeed, both RT-PCR and Northern blot analysis of spermatogonia, spermatocytes, round spermatids and elongated spermatids isolated by staput velocity sedimentation showed strong expression of ABCA17 mRNA. Immunoperoxidase staining with ABCA17 antibody confirmed that, with the exception of round spermatids, protein is present in spermatogonia, spermatocytes and elongated spermatids. The observation of ABCA17 transcripts and protein in spermatogonia has not been reported before and suggests that ABCA17 may play an important role during spermatogonial differentiation.

The immunoperoxidase staining technique used in this study is based on polymer intensification of reaction product which allows detection of very low levels of antigen. This contrasts to the immunofluoresent staining procedure which is essentially one antigen-to-one antibody reaction. The finding that only elongated spermatids were reactive by immunofluoresence is consistent with the likelihood that these cells contain much higher amounts of translated protein than do spermatocytes or spermatogonia. The presence of high levels of ABCA17 transcripts in round spermatids and high expression of ABCA17 protein in elongated spermatids and spermatozoa raises the possibility that the ABCA17 mRNA is posttranscriptionally regulated during spermiogenesis. Indeed, a number of testis-specific mRNAs are maximally transcribed in round spermatids at mid steps of spermiogenesis, although the peak amounts of proteins are synthesized days later in late elongated spermatids (Kleene et al., 1984; Hecht, 1989; El-Alfy et al., 1999; Morales et al., 2002). Therefore, it is entirely possible that the synthesis of mouse ABCA17 protein in late spermatids occurs long after the cessation of transcription in round spermatids.

Using Northern blot analysis, the present study showed that ABCA17 mRNA was expressed in testis at postnatal day 5, with expression gradually increasing at postnatal day 25 and postnatal day 45. The period of maximal ABCA17 mRNA expression corresponded to the time point when germ cells were fully differentiated. Immunoblotting of testicular lysates reacted with ABCA17 antibody showed low levels of protein expression at postnatal day 5 correlating with the presence of spermatogonia. At postnatal day 20, ABCA17 protein expression increased substantially, corresponding to the developmental appearance of pachytene spermatocytes. The level of protein further increased in the testis at postnatal day 45, consistent with the presence of elongated spermatids and spermatozoa. Thus, these results validated our observations on ABCA17 expression obtained on isolated germ cells.

Unlike ABCA1, ABCA7 and ABCG1 reported before by us in the sperm plasma membrane, ABCA17 is the first testis-specific transporter with a distinct topographical distribution. In addition to its presence in the mouse testis noted in the present study, ABCA17 has been found in rat testis (Ban et al., 2005) but its subcellular localization is presently unknown. Our studies show that ABCA17 is expressed differently in two important regions of the spermatozoa, the posterior region of the head and the mid piece of the tail. This unique distribution of ABCA17 may correlate with regionally distinct responses to lipid acceptor treatments such as the induction of acrosome reaction and motility. It is interesting to note that treatment of spermatozoa with the lipid acceptor albumin is known to alter the lipid composition of the plasma membrane with respect to distinct structural and functional regions of the sperm (Wolf et al., 1986). These changes are suspected to play a major role in the induction of acrosome reaction and hyperactivation of flagellar activity (Wolf et al., 1986).

In humans, the rodent Abca17 gene is a ubiquitously expressed pseudogene (ABCA17P). Interestingly, ABCA17P overlaps with the gene for the lung surfactant regulator ABCA3, and sequence homology analyses strongly suggest that ABCA3 is the progenitor gene of ABCA17P. In fact ABCA17 has 55.3% amino acid identity with ABCA3 (Ban et al., 2005; Piehler et al., 2006). In addition, an Abca3-like gene in the sea urchin genome, suABCA, is expressed in sperm and appears to be involved in shedding of cholesterol during sperm head maturation (Mengerink and Vacquier, 2002).

In the present study, we have obtained strong evidence indicating that ABCA17 is involved in sperm cholesterol efflux. The combination of NP40 and ABCA17 antibody produced a 40% inhibition of cholesterol efflux to lipid acceptor apoAI in sperm isolated from the corpus epididymidis. No effect was observed in sperm from the caput or cauda epididymidis. This inhibition was further increased when sperm were incubated in a cocktail containing both anti-ABCA17 and anti-ABCG1 antibodies. In fact, the combination of both antibodies produced a statistical significant inhibition of cholesterol efflux at the level of 25% in the corpus and 40% in the cauda epididymidis that was mainly attributed to the blockage of ABCG1. However, we cannot discard the possibility that both ABC

molecules operate synergistically.

Our findings indicate that ABCA17 mediated cholesterol efflux occurs exclusively in spermatozoa isolated from the corpus epididymis in presence of ApoA-I. Interestingly, ABCA1, ABCA7 and ABCG1 have also been shown to function in a regional specific manner in the epididymis (Morales et al., 2008). The physiological significance of the regional activity of the ABC transporters suggests that spermatozoa membrane remodelling takes place gradually during their maturation in the epididymis. The modification of spermatozoa cholesterol content during epididymal maturation has been investigated in several mammals, and a significant decrease of about 50% has been reported in ram, rat, hamster and mouse (reviewed by Saez et al., 2011). The cholesterol loss is usually accompanied by a decrease in the cholesterol/ phospholipids ratio, an indicator of membrane fluidity, suggesting that spermatozoa increase their membrane fluidity as the sperm transit through the epididymis (reviewed by Saez et al., 2011). In the goat, however, the spermatozoa cholesterol content increases during epididymal maturation, whereas in boar, no significant changes were noticed (reviewed by Saez et al., 2011). Although little is known about the content of cholesterol in the plasma membrane of human spermatozoa, the fluidity of cauda epididymal sperm was shown to be higher than the one from caput epididymal sperm, suggesting a decrease in cholesterol content (reviewed by Saez et al., 2011).

In summary, the ABC transporter, ABCA17, is expressed on the head and flagellar midpiece of mouse spermatozoa. Treatment of spermatozoa with anti-ABCA17 antibody reduces cholesterol efflux to lipid acceptors suggesting that this transporter plays a role in the process of sterol efflux. The latter activity may render spermatozoa capable of interacting with an oocyte by inducing the acrosome reaction and hyperactivated motility that leads to fertilization.

References

Argraves W.S. and Morales C.R. (2004). Immunolocalization of cubilin, megalin, apolipoprotein J, and apolipoprotein A-I in the uterus and oviduct. Mol. Reprod. Dev. 69, 419-427.

Ban N., Sasaki M., Sakai H., Ueda K. and Inagaki N. (2005). Cloning of ABCA17, a novel rodent sperm-specific ABC (ATP-binding cassette) transporter that regulates intracellular lipid metabolism. Biochem. J. 389, 577-585.

Benoff S. (1993). Preliminaries to fertilization. The role of cholesterol during capacitation of human spermatozoa. Hum. Reprod. 8, 2001-2006.

Beyea M.M., Heslop C.L., Sawyez C.G., Edwards J.Y., Markle J.G., Hegele R.A. and Huff M.W. (2007). Selective up-regulation of LXR-regulated genes ABCA1, ABCG1, and APOE in macrophages through increased endogenous synthesis of 24(S),25-epoxycholesterol. J. Biol. Chem. 282, 5207-5216.

Biemans-Oldehinkel E., Mahmood N.A. and Poolman B. (2006). A sensor for intracellular ionic strength. Proc. Natl. Acad. Sci. U S A. 103, 10624-10629.

Bortnick A.E., Rothblat G.H., Stoudt G., Hoppe K.L., Royer L.J., McNeish J. and Francone O.L. (2000). The correlation of ATP-binding cassette 1 mRNA levels with cholesterol efflux from various cell lines. J. Biol. Chem. 275, 28634-28640.

Cross N.L. (1998). Role of cholesterol in sperm capacitation. Biol. Reprod. 59, 7-11.

Cross N.L. and Razy-Faulkner P. (1997). Control of human sperm intracellular pH by cholesterol and its relationship to the response of the acrosome to progesterone. Biol. Reprod. 56, 1169-1174.

Davidson A.L. and Maloney P.C. (2007). ABC transporters: how small machines do a big job. Trends Microbiol. 15, 448-455.

Davis B.K. (1981). Timing of fertilization in mammals: sperm cholesterol/phospholipid ratio as a determinant of the capacitation interval. Proc. Natl. Acad. Sci. USA 78, 7560-7564.

Dawson R.J., Hollenstein K. and Locher K.P. (2007). Uptake or extrusion: crystal structures of full ABC transporters suggest a common mechanism. Mol. Microbiol. 65, 250-257.

Dean M., Rzhetsky A. and Allikmets R. (2001). The human ATP-binding cassette (ABC) transporter superfamily. Genome Res. 11, 1156-1166.

El-Alfy M., Moshonas D., Morales C.R. and Oko R. (1999). Molecular cloning and developmental expression of the major fibrous sheath protein (FS 75) of rat sperm. J. Androl. 20, 307-318.

Gottesman M.M., Fojo T. and Bates S.E. (2002). Multidrug resistance in cancer: role of ATP-dependent transporters. Nat. Rev. Cancer 2, 48-58.

Hecht N.B. (1989). Structural DNA-binding proteins of the testis. In: Molecular biology of chromosome function. Adolph K.W. (ed). Springer-Verlag. New York. pp 396-420.

Hermo L., Wright J., Oko R. and Morales C.R. (1991). Role of epithelial cells of the male excurrent duct system of the rat in the endocytosis or secretion of sulfated glycoprotein-2 (clusterin). Biol. Reprod. 44, 1113-1131.

Hermo L., Schellenberg M., Liu L.Y., Dayanandan B., Zhang T., Mandato C.A. and Smith C.E. (2008). Membrane domain specificity in the spatial distribution of aquaporins 5, 7, 9, and 11 in efferent ducts and epididymis of rats. J. Histochem. Cytochem. 56, 1121-1135.

Hermo L., Pelletier R.M., Cyr D.G. and Smith C.E. (2010). Surfing the wave, cycle, life history, and genes/proteins expressed by testicular germ cells. Part 5: intercellular junctions and contacts between germs cells and Sertoli cells and their regulatory interactions, testicular cholesterol, and genes/proteins associated with more than one germ cell generation. Microsc. Res. Tech., 73, 409-494.

Higgins C.F. (1992). ABC transporters: from microorganisms to man. Annu. Rev. Cell Biol. 8, 67-113.

Hollenstein K., Dawson R.J. and Locher K.P. (2007a). Structure and mechanism of ABC transporter proteins. Curr. Opin. Struct .Biol. 17, 412-418.

Hollenstein K., Frei D.C. and Locher K.P. (2007b). Structure of an ABC transporter in complex with its binding protein. Nature 446, 213-216.

Jaspard B., Collet X., Barbaras R., Manent J., Vieu C., Parinaud J., Chap H. and Perret B. (1996). Biochemical characterization of pre-beta 1 high-density lipoprotein from human ovarian follicular fluid: evidence for the presence of a lipid core. Biochemistry 35, 1352-1357.

Jones P.M. and George A.M. (2004). The ABC transporter structure and mechanism: perspectives on recent research. Cell Mol. Life Sci. 61, 682-699.

Jones R. (1998). Plasma membrane structure and remodelling during sperm maturation in the epididymis. J. Reprod. Fertil. Suppl. 53, 73-84.

Kleene K.C., Distel R.J. and Hecht N.B. (1984). Translational regulation and deadenylation of a protamine mRNA during spermiogenesis in the mouse. Dev. Biol. 105, 71-79.

Klein I., Sarkadi B. and Varadi A. (1999). An inventory of the human ABC proteins. Biochim. Biophys. Acta 1461, 237-262.

Koshiba S., An R., Saito H., Wakabayashi K., Tamura A. and Ishikawa T. (2008). Human ABC transporters ABCG2 (BCRP) and ABCG4. Xenobiotica 38, 863-888.

Lassalle B., Bastos H., Louis J.P., Riou L., Testart J., Dutrillaux B., Fouchet P. and Allemand I. (2004). Side Population' cells in adult mouse testis express Bcrp1 gene and are enriched in spermatogonia and germinal stem cells. Development 131, 479-487.

Law G.L., McGuinness M.P., Linder C.C. and Griswold M.D. (1997). Expression of apolipoprotein E mRNA in the epithelium and interstitium of the testis and the epididymis. J. Androl. 18, 32-42.

Lybaert P., Vanbellinghen A.M., Quertinmont E., Petein M., Meuris S. and Lebrun P. (2008). KATP channel subunits are expressed in the epididymal epithelium in several mammalian species. Biol. Reprod. 79, 253-261.

Martinez P. and Morros A. (1996). Membrane lipid dynamics during human sperm capacitation. Front. Biosci. 1, d103-117.

Mengerink K.J. and Vacquier V.D. (2002). An ATP-binding cassette transporter is a major glycoprotein of sea urchin sperm membranes. J. Biol. Chem. 277, 40729-40734.

Morales C.R., Igdoura S.A., Wosu U.A., Boman J. and Argraves W.S. (1996). Low density lipoprotein receptor-related protein-2 expression in efferent duct and epididymal epithelia: evidence in rats for its in vivo role in endocytosis of apolipoprotein J/clusterin. Biol. Reprod. 55, 676-683.

Morales C.R., Lefrancois S., Chennathukuzhi V., El-Alfy M., Wu X., Yang J., Gerton G.L. and Hecht N.B. (2002). A TB-RBP and Ter ATPase complex accompanies specific mRNAs from nuclei through the nuclear pores and into intercellular bridges in mouse male germ cells. Dev. Biol. 246, 480-494.

Morales C.R., Marat A.L., Ni X., Yu Y., Oko R., Smith B.T. and Argraves W.S. (2008). ATP-binding cassette transporters ABCA1, ABCA7, and ABCG1 in mouse spermatozoa. Biochem. Biophys. Res. Commun. 376, 472-477.

Oldham M.L., Davidson A.L. and Chen J. (2008). Structural insights into ABC transporter mechanism. Curr. Opin. Struct. Biol. 18, 726-733.

Ouvrier A., Cadet R., Vernet P., Laillet B., Chardigny J.M., Lobaccaro J.M., Drevet J.R. and Saez F. (2009). LXR and ABCA1 control cholesterol homeostasis in the proximal mouse epididymis in a cell-specific manner. J. Lipid Res. 50, 1766-1775.

Petrie R.G. and Morales C.R. (1992). Receptor-mediated endocytosis of testicular transferrin by germinal cells of the rat testis. Cell Tissue Res. 267, 45-55.

Piehler A.P., Wenzel J.J., Olstad O.K., Haug K.B., Kierulf P. and Kaminski W.E. (2006). The human ortholog of the rodent testis-specific ABC transporter Abca17 is a ubiquitously expressed pseudogene (ABCA17P) and shares a common 5' end with ABCA3. BMC Mol. Biol. 7, 28.

Potocnik U., Glavac D. and Dean M. (2008). Common germline MDR1/ABCB1 functional polymorphisms and haplotypes modify susceptibility to colorectal cancers with high microsatellite instability. Cancer Genet. Cytogenet. 183, 28-34.

Robaire B. and Henderson N.A. (2006). Actions of 5alpha-reductase inhibitors on the epididymis. Mol. Cell. Endocrinol. 250, 190-195.

Robaire B. and Hermo L. (1988). Efferent ducts, epididymis and vas deferens: structure, functions and their regulation. In: The physiology of reproduction. Vol. 1. Neil J.D. (ed). Raven Press. New York. pp 999-1080.

Saez F., Ouvrier A. and Drevet J.R. (2011). Epididymis cholesterol homeostasis and sperm fertilizing ability. Asian J. Androl. 13, 11-17.

Selva D.M., Hirsch-Reinshagen V., Burgess B., Zhou S., Chan J., McIsaac S., Hayden M.R., Hammond G.L., Vogl A.W. and Wellington C.L. (2004). The ATP-binding cassette transporter 1 mediates lipid efflux from Sertoli cells and influences male fertility. J. Lipid Res. 45, 1040-1050.

Shadan S., James P.S., Howes E.A. and Jones R. (2004). Cholesterol efflux alters lipid raft stability and distribution during capacitation of boar spermatozoa. Biol. Reprod. 71, 253-265.

Scharenberg C., Mannowetz N., Robey R.W., Brendel C., Repges P., Sahrhage T., Jähn T. and Wennemuth G. (2009). ABCG2 is expressed in late spermatogenesis and is associated with the acrosome. Biochem. Biophys. Res. Commun. 378, 302-307.

Sylvester S.R., Morales C., Oko R. and Griswold M.D. (1991). Localization of sulfated glycoprotein-2 (clusterin) on spermatozoa and in the reproductive tract of the male rat. Biol. Reprod. 45, 195-207.

Travis A.J. and Kopf G.S. (2002). The role of cholesterol efflux in regulating the fertilization potential of mammalian spermatozoa. J. Clin. Invest. 110, 731-736.

Turner T.T. and Bomgardner D. (2002). On the regulation of Crisp-1 mRNA expression and protein secretion by luminal factors presented in vivo by microperfusion of the rat proximal caput epididymidis. Mol. Reprod. Dev. 61, 437-444.

Van Praet O., Argraves W.S. and Morales C.R. (2003). Co-expression and interaction of cubilin and megalin in the adult male rat reproductive system. Mol. Reprod. Dev. 64, 129-135.

Váradi A T.G. and Sarkadi B. (2003). Membrane topology of the human ABC transporter proteins. In: ABC proteins: from bacteria to man. Holland I.B., Cole S.P.C., Kuchler K. and Higgins C.F. (eds). Academic Press. Amsterdam. pp 37-46.

Velamakanni S., Wei S.L., Janvilisri T. and van Veen H.W. (2007). ABCG transporters: structure, substrate specificities and physiological roles: a brief overview. J. Bioenerg. Biomembr. 39, 465-471.

Visconti P.E., Moore G.D., Bailey J.L., Leclerc P., Connors S.A., Pan D., Olds-Clarke P. and Kopf G.S. (1995). Capacitation of mouse spermatozoa. II. Protein tyrosine phosphorylation and capacitation are regulated by a cAMP-dependent pathway. Development 121, 1139-1150.

Visconti, P.E. Galantino-Homer H., Ning X., Moore G.D., Valenzuela J.P., Jorgez C.J., Alvarez J.G. and Kopf G.S. (1999). Cholesterol efflux-mediated signal transduction in mammalian sperm. ,-cyclodextrins initiate transmembrane signaling leading to an increase in protein tyrosine phosphorylation and capacitation. J. Biol. Chem. 274, 3235-3242.

Wang N., Lan D., Chen W., Matsuura F. and Tall A.R. (2004). ATP-

binding cassette transporters G1 and G4 mediate cellular cholesterol efflux to high-density lipoproteins. Proc. Natl. Acad. Sci. USA 101, 9774-9779.

Wolf D.E., Hagopian S.S. and Ishijima S. (1986). Changes in sperm plasma membrane lipid diffusibility after hyperactivation during in vitro capacitation in the mouse. J. Cell Biol. 102, 1372-1377.

Accepted October 7, 2011

ORIGINAL ARTICLE

Effects of glucose and meal ingestion on incretin secretion in Japanese subjects with normal glucose tolerance

Shunsuke Yamane, Norio Harada, Akihiro Hamasaki, Atsushi Muraoka, Erina Joo, Kazuyo Suzuki, Daniela Nasteska, Daisuke Tanaka, Masahito Ogura, Shin-ichi Harashima, Nobuya Inagaki*

ABSTRACT

Aims/Introduction: Gastric inhibitory polypeptide (GIP) and glucagon-like peptide-1 (GLP-1) are the major incretins; their secretion after various nutrient loads are well-evaluated in Caucasians. However, little is known of the relationship between incretin secretion and differing nutritional loading in Japanese subjects. In the present study, we evaluated GIP and GLP-1 secretion in Japanese subjects with normal glucose tolerance (NGT) after glucose loading (75 g glucose and 17 g glucose) and meal ingestion.

Materials and Methods: A total of 10 Japanese NGT subjects participated in 75 g oral glucose tolerance test (OGTT), 17 g OGTT and meal tolerance test (MTT). Plasma glucose (PG), serum insulin (IRI), serum C-peptide (CPR), plasma total GIP, and plasma total GLP-1 levels during OGTT and MTT were determined.

Results: Area under the curve (AUC)-GIP was increased in proportion to the amount of glucose, and was highest in MTT, showing that GIP secretion is also stimulated by nutrients other than glucose, such as lipid. In contrast, although the larger glucose load tended to induce a larger GLP-1 release, AUC-GLP-1 was not significantly different among the three loading tests (75 g OGTT, 17 g OGTT, MTT) irrespective of the kind or amount of nutrition load.

Conclusions: Our results suggest that nutritional composition might have a greater effect on GIP secretion than that on GLP-1 secretion in Japanese NGT subjects. (J Diabetes Invest, doi: 10.1111/j.2040-1124.2011.00143.x, 2012)

KEY WORDS: Incretin, Meal tolerance test, Oral glucose tolerance test

INTRODUCTION

Oral glucose administration leads to greater insulin release from pancreatic islets than that by intravenous glucose loading yielding equivalent glucose levels. Gut hormonal substances released in response to glucose include the incretins, gastric inhibitory polypeptide (GIP) and glucagon-like peptide-1 (GLP-1), which are responsible for 50–60% of postprandial insulin secretion[1]. GIP is secreted on meal ingestion from K-cells in the proximal small intestine, whereas GLP-1 is secreted from L-cells in the distal small intestine and colon, and binds to their respective receptors on the surface of pancreatic β-cells to stimulate insulin secretion by increasing the intracellular adenosine 3′,5′-monophosphate concentration[2].

The incretin effect has been shown to be reduced in type 2 diabetic patients compared with that in normal glucose tolerance (NGT) subjects in previous studies[3,4], suggesting that a reduced incretin effect might be associated with hyperglycemia after food intake and glucose loading in type 2 diabetes. Plasma GLP-1 concentrations in type 2 diabetic patients have been reported to be reduced after meal ingestion and glucose loading[4,5]. However, in other studies, it was reported that GLP-1 concentrations did not differ in NGT and type 2 diabetic patients[6–8]. When intravenous infusion of GIP or GLP-1 was carried out in type 2 diabetic patients, GLP-1 potentiated insulin secretion from pancreatic β-cells, but GIP did not, showing that the GIP receptor (GIPR) signal is reduced in β-cells in type 2 diabetes[9]. In contrast, the GIPR signal plays an important role in maintaining blood glucose levels in the non-diabetic obese state[10,11]. Indeed, GIP concentrations are reported to be increased in obese rodent models and obese Caucasian subjects compared with those in lean rodents and lean Caucasian subjects, respectively[12–14]. In addition, we have previously shown hypersensitivity of GIPR to GIP in β-cells of high fat-induced obese mice[11]. In summary, evaluation of incretin secretion and the incretin effect in subjects with various levels of glucose tolerance is important to determine the contribution of incretin deficiency in progression from NGT to type 2 diabetes.

Type 2 diabetes is characterized by both decreased insulin secretion and reduced insulin sensitivity[15–17]. In Caucasians,

Department of Diabetes and Clinical Nutrition, Graduate School of Medicine, Kyoto University, Kyoto, Japan
*Corresponding author. Nobuya Inagaki Tel.: +81-75-751-3560 Fax: +81-75-751-4244
E-mail address: inagaki@metab.kuhp.kyoto-u.ac.jp
Received 24 March 2011; revised 25 April 2011; accepted 16 May 2011

insulin resistance is thought to play a critical role in the pathogenesis of type 2 diabetes. In contrast, insulin sensitivity in Asian subjects has been shown to be higher than that in Mexican Americans and Caucasians in previous reports[18,19], which is partly because of the fact that Asians, including Japanese, are generally less obese. Thus, insulin secretion rather than insulin sensitivity is considered to be the more important factor in progression from NGT to diabetes in Japanese subjects[20]. Indeed, we have reported that early-phase insulin secretion is considerably decreased even in Japanese NGT subjects with 1-h plasma glucose levels higher than 10 mmol/L during an oral glucose tolerance test (OGTT)[21].

A recent study showed that, in both Caucasian NGT subjects and Caucasian type 2 diabetic patients, a meal tolerance test (MTT) elicited a significantly greater response of GIP levels than that elicited by OGTT, whereas GLP-1 levels were not different between OGTT and MTT[6]. In a previous study comparing the incretin secretion measured after different amounts of glucose load in healthy Caucasian subjects and type 2 diabetic Caucasian patients, GLP-1 and GIP were dose-dependently increased[22]. Plasma GLP-1 and GIP levels after glucose load or meal ingestion have been evaluated mainly in Caucasian subjects. In Japanese subjects, there has not been thorough elucidation, and little is known about the relationship between incretin secretion, and the kind and amount of nutrition load.

In the present study, we investigated incretin levels in association with the amount of glucose load and meal ingestion by measuring plasma GLP-1 and GIP levels after administration of 17 or 75 g glucose or mixed meal in Japanese NGT subjects.

MATERIALS AND METHODS

Subjects

A total of 10 healthy Japanese volunteers (eight male and two female) were recruited into the present study. The subjects had no history of hypertension, hyperlipidemia or kidney and liver diseases, and did not take any drugs 2 weeks before the study. The study was designed in compliance with the ethics regulations of the Helsinki Declaration and Kyoto University. Informed consent was obtained from all subjects.

Study Procedure

The subjects' age, height and bodyweight were determined. Blood samples for measurement of liver and kidney function, HbA_{1c} (National Glycohemoglobin Standardization Program), triglycerides (TG), total cholesterol and high-density lipoprotein (HDL)-cholesterol levels were drawn after an overnight fast. All subjects received 75 g OGTT, 17 g (approximately a quarter of 75 g) OGTT and a MTT. The interval between tests was 2–4 weeks. The total caloric content of the test meal was 450 kcal (carbohydrates 57.8 g, protein 17.2 g, fat 16.6 g). After the subjects fasted overnight for 10–16 h, OGTT or MTT was carried out according to the National Diabetes Data Group recommendations[23]. NGT was diagnosed according to World Health Organization (WHO) criteria[24].

Blood samples were collected at 0, 30, 60, 120 and 180 min after glucose loadings or meal ingestion and were centrifuged at 1800 *g* at 4°C for 10 min. After collecting supernatant of the samples, plasma and serum were stocked at −80°C. Blood was distributed into chilled tubes containing ethylenediaminetetraacetic acid and aprotinin (500 kIU/mL blood, Trasylol; SRL Inc., Tokyo, Japan) for analyses of GLP-1 and GIP. Plasma glucose (PG), serum insulin (IRI), serum C-peptide (CPR), plasma total GIP and plasma total GLP-1 were measured at the indicated times. The PG levels were measured by the glucose oxidase method. Serum IRI and CPR levels were measured by enzyme-linked immunosorbent assay. Total GIP and total GLP-1 levels were measured using a human GIP ELISA kit (Linco Research, St Charles, MO, USA) and human GLP-1 ELISA kit (Meso Scale Discovery, Gaithersburg, MD, USA), respectively, as previously described[25].

Calculations and Statistical Analysis

The area under the curve of PG (AUC-PG), IRI (AUC-IRI), CPR (AUC-CPR), total GIP (AUC-GIP) and total GLP-1 (AUC-GLP-1) were calculated by the trapezoidal rule. Statistical analyses were carried out using ANOVA and unpaired Student's *t*-test. *P*-values <0.05 were considered statistically significant. Data are presented as mean ± standard error (SE).

RESULTS

The profiles of the subjects are shown in Table 1. Mean age was 32.2 ± 2.0 years and mean body mass index was 22.4 ± 0.8 kg/m^2. Insulinogenic index, homeostasis model assessment (HOMA)-β and HOMA-insulin resistance were 0.59 ± 0.10, 76.50 ± 12.60, 1.10 ± 0.19, respectively. No subjects had liver or kidney dysfunction. HbA_{1c}, PG, TG, total cholesterol and HDL-cholesterol levels were within normal limits in the fasting state.

The profiles of PG, IRI and CPR in 75 g OGTT, 17 g OGTT and MTT are shown in Figure 1. Judging by the results of 75 g OGTT, all the subjects were diagnosed with NGT according to WHO criteria with fasting plasma glucose and 2 h glucose levels below 6.1 and 7.8 mmol/L, respectively. Fasting concentrations of PG, IRI and CPR were not different among the two OGTT and

Table 1 | Clinical characteristics of the subjects

n (Male/female)	10 (8/2)
Age (years)	32.2 ± 2.0
BMI (kg/m^2)	22.4 ± 0.8
Fasting plasma glucose (mmol/L)	4.9 ± 0.2
HbA_{1c} (%)	5.3 ± 0.1
Triglycerides (mg/dL)	79.4 ± 10.5
Total cholesterol (mg/dL)	169.2 ± 6.1
HDL-cholesterol (mg/dL)	61.5 ± 5.3
LDL-cholesterol (mg/dL)	93.0 ± 9.2

Data represent the mean ± SD. BMI, body mass index; HDL, high-density lipoprotein; LDL, low-density lipoprotein.

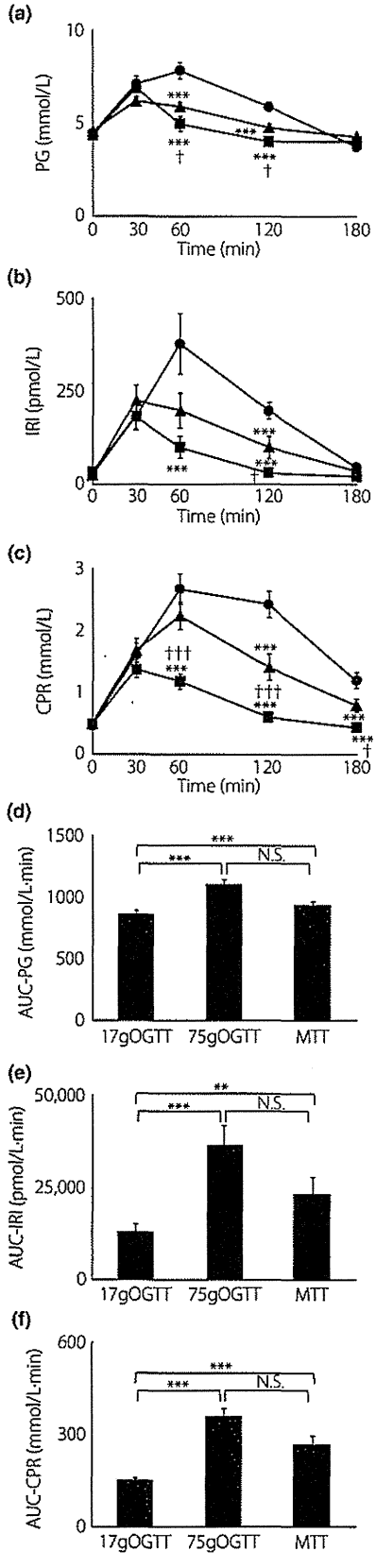

Figure 1 | Concentrations of (a) plasma glucose (PG), (b) serum insulin (IRI) and (c) serum C-peptide (CPR) during the 75 g oral glucose tolerance test (OGTT; closed circle), 17 g OGTT (closed square) and meal tolerance test (MTT; closed triangle) in 10 Japanese subjects. Asterisks indicate significant differences vs 75 g OGTT at individual time-points (*P < 0.05, **P < 0.01, ***P < 0.001); daggers indicate significant differences vs MTT at individual time-points (†P < 0.05, ††P < 0.01, †††P < 0.001). (d) Area under the curve (AUC)-PG, (e) AUC-IRI, (f) AUC-CPR were calculated by the trapezoidal rule. Asterisks indicate significant differences at individual time-points (*P < 0.05, **P < 0.01, ***P < 0.001). Statistical analyses were carried out using ANOVA and unpaired Student's t-test. P-values <0.05 were considered statistically significant. Data are presented as mean ± standard error. N.S., not significant.

MTT. In OGTT studies, AUC-PG, AUC-IRI and AUC-CPR measured by the 75 g OGTT were significantly larger than those measured by the 17 g OGTT (Figure 1d–f). At 30 min after glucose ingestion, the levels of PG, IRI and CPR in the 75 g OGTT and those in the 17 g OGTT were not significantly different. Between MTT and the two OGTT, AUC-PG, AUC-IRI and AUC-CPR in MTT were significantly higher than those in the 17 g OGTT. AUC-PG, AUC-IRI and AUC-CPR in the 75 g OGTT and in MTT were not significantly different.

In the 17 g OGTT, the total GLP-1 level peaked at 30 min and rapidly decreased to the baseline at 60 min after the glucose load. The total GLP-1 level peaked at 30 min after the meal load and was sustained for up to 180 min. In the 75 g OGTT, the GLP-1 level peaked at 60 min and gradually decreased with time, but the level was still higher than baseline even at 180 min. The level of total GLP-1 at 60 min after the 75 g glucose load was significantly higher than that after the 17 g glucose load (Figure 2a). Although a larger glucose load tended to induce a larger GLP-1 release, total AUC-GLP-1 measured by the 75 g OGTT, 17 g OGTT and MTT were not significantly different (Figure 2b).

The baseline levels of GIP were approximately 10 pmol/L. The GIP level rapidly increased, peaked at 30 min after the meal load and gradually decreased with time, but the level was still higher than baseline even at 180 min. In the 75 g OGTT, the GIP level significantly increased at 30 min after the glucose load, peaked at 120 min and were maintained up to 180 min. In the 17 g OGTT, the total GIP level peaked at 30 min after glucose load and gradually decreased to baseline at 180 min. At 30 min after ingestion, total GIP levels in the 75 g OGTT and those in the 17 g OGTT were not significantly different (Figure 3a).

AUC-GIP was significantly higher in the 75 g OGTT than that in the 17 g OGTT. Unlike GLP-1, the peak levels of GIP and the AUC-GIP measured in the MTT were significantly higher than those measured in the 75 g OGTT and 17 g OGTT (Figure 3b).

DISCUSSION

In the present study, incretin levels were estimated after glucose loading or meal ingestion in Japanese NGT subjects.

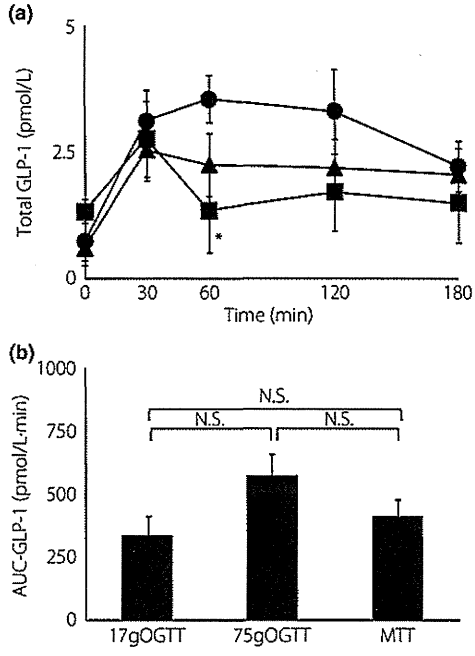

Figure 2 | (a) Concentrations of total glucagon-like peptide-1 (GLP-1) during the 75 g oral glucose tolerance test (OGTT; closed circle), 17 g OGTT(closed square) and meal tolerance test (MTT; closed triangle) in 10 Japanese subjects. Asterisks indicate significant differences vs 75 g OGTT at individual time-points (*P < 0.05, **P < 0.01, ***P < 0.001); daggers indicate significant differences vs MTT at individual time-points (†P < 0.05, ††P < 0.01, †††P < 0.001). (b) Area under the curve (AUC)-GLP-1 was calculated by the trapezoidal rule. Asterisks indicate significant differences at individual time-points (*P < 0.05, **P < 0.01, ***P < 0.001). Statistical analyses were carried out using ANOVA and unpaired Student's t-test. P-values <0.05 were considered statistically significant. Data are presented as mean ± standard error. N.S., not significant.

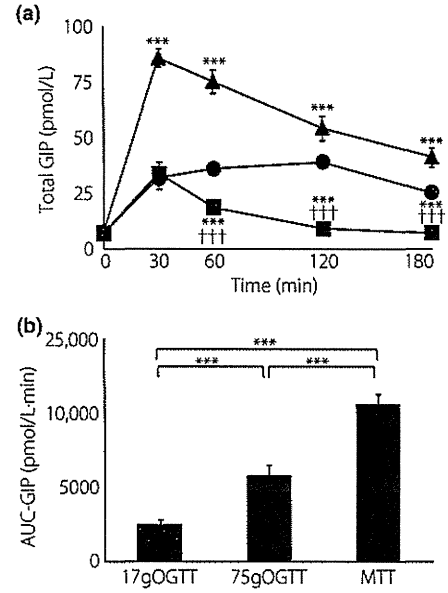

Figure 3 | (a) Concentrations of total gastric inhibitory polypeptide (GIP) during 75 g oral glucose tolerance test (OGTT; closed circle), 17 g OGTT (closed square) and meal tolerance test (MTT; closed triangle) in 10 Japanese subjects. Asterisks indicate significant differences vs 75 g OGTT at individual time-points (*P < 0.05, **P < 0.01, ***P < 0.001); daggers indicate significant differences vs MTT at individual time-points (†P < 0.05, ††P < 0.01, †††P < 0.001). (b) Area under the curve (AUC)-GIP was calculated by the trapezoidal rule. Asterisks indicate significant differences at individual time-points (*P < 0.05, **P < 0.01, ***P < 0.001). Statistical analyses were carried out using ANOVA and unpaired Student's t-test. P-values <0.05 were considered statistically significant. Data are presented as mean ± standard error.

Between the OGTT studies, AUC-PG, AUC-IRI and AUC-CPR in the 75 g OGTT were larger than those in the 17 g OGTT. Regarding incretins, AUC-GIP was significantly larger in the 75 g OGTT than in the 17 g OGTT. In contrast, AUC-GLP-1 was not significantly different between the 75 g OGTT and the 17 g OGTT. Previous studies showed that a larger amount of oral glucose load elicited more GIP and GLP-1 secretion[1,22], whereas a recent study also reported that the secretory response of GIP was more sensitive than that of GLP-1 to changes in intestinal carbohydrate content[26]. The present study also showed that while GLP-1 level was not increased, GIP level was increased dose-dependently in response to glucose load, showing higher sensitivity of GIP to changes of administered nutrient dose.

Between the 75 g OGTT and MTT studies, AUC-PG, AUC-IRI and AUC-CPR were not significantly different. AUC-GIP was significantly larger in MTT than that in the 75 g OGTT. In contrast, there was no significant difference in AUC-GLP-1 among the MTT and the two OGTT. By comparing the results of the three loading tests (75 g OGTT, 17 g OGTT, MTT), we speculate that AUC-GIP is more susceptible to the contents of each loading test than AUC-GLP-1 is. Vollmer *et al.*[6] reported that GIP responses were significantly higher in MTT than in OGTT, whereas GLP-1 levels were similar in both tests in Caucasian NGT, IGT and type 2 diabetic subjects. Because the mixed meal contains not only carbohydrates but also fat, which has been reported to stimulate GIP secretion[27–29], it is likely that the increased GIP concentrations after MTT were largely as a result of the fat content, which might have had no additional impact on GLP-1 secretion.

There are two previous reports that evaluate the incretin levels in both OGTT and MTT in Japanese NGT subjects[8,30]. However, they compared the incretin levels in 75 g glucose or meal load between NGT and type 2 diabetic subjects, but did not compare the incretin levels between 75 g glucose and meal load directly. The present study directly compared the incretin levels in the two OGTT and MTT. Our data clearly show that GIP responses were significantly higher in MTT than those in the two OGTT, whereas GLP-1 levels were not different between the two OGTT and MTT in Japanese NGT subjects.

According to the study by Yabe *et al.*[8], AUC-GIP is similar between the OGTT and MTT group in Japanese control subjects. It should be noted that the difference between GIP secretion after meal load and that after glucose load was far greater in the present study than that in the study by Yabe *et al.* The total caloric content of the test meal used in their study was 480 kcal (carbohydrates 58.4%, protein 20.8%, fat 20.8%) and that in the present study was 450 kcal (carbohydrates 51.4%, protein 15.3%, fat 33.3%). Therefore, it is possible that the higher amount of contained fat in the test meal used in the present study led to the greater response of GIP secretion in the MTT.

Fasting and peak total GLP-1 concentrations in the present study were approximately 1 pmol/L and 3.5 pmol/L, respectively, and seemed to be lower than those in some published results[8,31]. However, in other reports, total GLP-1 levels after glucose and meal load were not very different from those in the present study. Rijkelijkhuizen *et al.*[32] measured the total GLP-1 concentration with radioimmunoassay, and in their results, the fasting and peak total GLP-1 concentrations in the MTT were approximately 1 pmol/L and 4.5 pmol/L, respectively. In addition, Villareal *et al.*[33] evaluated total GLP-1 concentrations by the same method that we used in the present study, and reported that the fasting and peak total GLP-1 concentrations in OGTT were approximately 1.5 and 6 pmol/L, respectively. Judging by the data in these reports, it is not necessarily the case that total GLP-1 concentrations were extremely low in the present study.

There are some reports showing that GLP-1 secretion is dependent on meal size, especially on carbohydrate and glucose loads. Schirra *et al.*[34] reported that GLP-1 plasma levels rose from basal levels to fourfold after 50 g glucose ingestion and to eightfold after 100 g glucose ingestion. Rijkelijkhuizen *et al.*[32] showed that GLP-1 secretion is increased by the amount of carbohydrate (75 and 109 g) and not by the quantity of the meal. In the present study, however, AUC-GLP-1 was not significantly different among the three loading tests (75 g OGTT, 17 g OGTT, MTT) irrespective of kinds or amounts of nutrition load, although larger glucose load tended to induce a larger GLP-1 release. The most notable difference between the previous studies and the present study was the amount of glucose load. We compared GLP-1 secretion after administration of 17 g glucose, 75 g glucose and 57.8 g of carbohydrate contained in the meal that we used. The amount of glucose and carbohydrate load in the present study were relatively lower than those in the previous studies. It is possible that evaluation of GLP-1 secretion after larger glucose loads could be more appropriate to show the glucose dependency of GLP-1 secretion.

It is also noteworthy that the levels of PG, IRI, CPR, GIP and GLP-1 at 30 min after the 75 g OGTT and 17 g OGTT were similar to each other. In addition, the levels of IRI, CPR and GLP-1 at 30 min after MTT and the two OGTT were not significantly different. By contrast, the GIP level at 30 min after MTT was much higher than those after the 17 g OGTT and 75 g OGTT. Given the similar plasma glucose levels at 30 min after the 17 g OGTT and 75 g OGTT, it is likely that under physiological conditions, the rate at which ingested glucose emptied into the duodenum is regulated finely enough to prevent an abrupt increase in plasma glucose levels irrespective of the amount of ingested glucose. Previous studies have shown that GLP-1 secretion after a test meal or oral glucose load is associated with the rate of gastric emptying, whereas GIP secretion seems to be dependent on nutrient absorption rather than on rate of gastric emptying[34]. Accordingly, a finely regulated rate of gastric emptying might account for the similar levels of GLP-1 at 30 min after MTT, 17 g OGTT and 75 g OGTT. In contrast, the level of total GIP at 30 min after the MTT was much higher than those after the two OGTT, probably because of the presence of fat in the duodenal lumen, as fat is a forcible stimulant of GIP, as discussed earlier.

The present results clearly show that the secretion of GIP and GLP-1 are regulated by different nutrient factors. On the basis of our data, it is also suggested that nutritional composition might have a greater effect on GIP secretion than on GLP-1 secretion in Japanese NGT subjects.

ACKNOWLEDGEMENTS

We thank Dr Yutaka Seino (Kansai Electric Power Hospital) for his helpful suggestions. This study was supported by Scientific Research Grants from the Ministry of Education, Culture, Sports, Science, and Technology of Japan, and by Kyoto University Global COE Program 'Center for Frontier Medicine', and also by Novo Nordisk Pharma Ltd.

REFERENCES

1. Nauck MA, Homberger E, Siegel EG, *et al.* Incretin effects of increasing glucose loads in man calculated from venous insulin and C-peptide responses. *J Clin Endocrinol Metab* 1986; 63: 492–498.
2. Seino Y, Fukushima M, Yabe D. GIP and GLP-1, the two incretin hormone: similarities and difference. *J Diabetes Invest* 2010; 1: 8–23.
3. Nauck M, Stockmann F, Ebert R, *et al.* Reduced incretin effect in type 2 (non-insulin-dependent) diabetes. *Diabetologia* 1986; 29: 46–52.
4. Muscelli E, Mari A, Casolaro A, *et al.* Separate impact of obesity and glucose tolerance on the incretin effect in normal subjects and type 2 diabetic patients. *Diabetes* 2008; 57: 1340–1348.
5. Vilsboll T, Krarup T, Deacon CF, *et al.* Reduced postprandial concentrations of intact biologically active glucagon-like peptide 1 in type 2 diabetic patients. *Diabetes* 2001; 50: 609–613.
6. Vollmer K, Holst JJ, Baller B, *et al.* Predictors of incretin concentrations in subjects with normal, impaired, and diabetic glucose tolerance. *Diabetes* 2008; 57: 678–687.
7. Faerch K, Vaag A, Holst JJ, *et al.* Impaired fasting glycaemia vs impaired glucose tolerance: similar impairment of pancreatic alpha and beta cell function but differential roles of incretin hormones and insulin action. *Diabetologia* 2008; 51: 853–861.

8. Yabe D, Kuroe A, Lee S, *et al.* Little enhancement of meal-induced glucagon-like peptide 1 secretion in Japanese: comparison of type 2 diabetes patients and healthy controls. *J Diabetes Invest* 2010; 1: 56–59.
9. Nauck MA, Heimesaat MM, Orskov C, *et al.* Preserved incretin activity of glucagon-like peptide 1 [7-36 amide] but not of synthetic human gastric inhibitory polypeptide in patients with type-2 diabetes mellitus. *J Clin Invest* 1993; 91: 301–307.
10. Miyawaki K, Yamada Y, Yano H, *et al.* Glucose intolerance caused by a defect in the entero-insular axis: a study in gastric inhibitory polypeptide receptor knockout mice. *Proc Natl Acad Sci USA* 1999; 96: 14843–14847.
11. Harada N, Yamada Y, Tsukiyama K, *et al.* A novel GIP receptor splice variant influences GIP sensitivity of pancreatic beta-cells in obese mice. *Am J Physiol Endocrinol Metab* 2008; 294: E61–E68.
12. Miyawaki K, Yamada Y, Ban N, *et al.* Inhibition of gastric inhibitory polypeptide signaling prevents obesity. *Nat Med* 2002; 8: 738–742.
13. Flatt PR, Bailey CJ, Kwasowski P, *et al.* Abnormalities of GIP in spontaneous syndromes of obesity and diabetes in mice. *Diabetes* 1983; 32: 433–435.
14. Creutzfeldt W, Ebert R, Willms B, *et al.* Gastric inhibitory polypeptide (GIP) and insulin in obesity: increased response to stimulation and defective feedback control of serum levels. *Diabetologia* 1978; 14: 15–24.
15. Mitrakou A, Kelley D, Mokan M, *et al.* Role of reduced suppression of glucose production and diminished early insulin release in impaired glucose tolerance. *N Engl J Med* 1992; 326: 22–29.
16. Haffner SM, Stern MP, Hazuda HP, *et al.* Increased insulin concentrations in nondiabetic offspring of diabetic parents. *N Engl J Med* 1988; 319: 1297–1301.
17. Saad MF, Knowler WC, Pettitt DJ, *et al.* A two-step model for development of non-insulin-dependent diabetes. *Am J Med* 1991; 90: 229–235.
18. Chiu KC, Chuang LM, Yoon C. Comparison of measured and estimated indices of insulin sensitivity and beta cell function: impact of ethnicity on insulin sensitivity and beta cell function in glucose-tolerant and normotensive subjects. *J Clin Endocrinol Metab* 2001; 86: 1620–1625.
19. Mandavilli A, Cyranoski D. Asia's big problem. *Nat Med* 2004; 10: 325–327.
20. Seino Y, Ikeda M, Yawata M, *et al.* The insulinogenic index in secondary diabetes. *Horm Metab Res* 1975; 7: 323–335.
21. Harada N, Fukushima M, Toyoda K, *et al.* Factors responsible for elevation of 1-h postchallenge plasma glucose levels in Japanese men. *Diabetes Res Clin Pract* 2008; 81: 284–289.
22. Bagger JI, Knop FK, Lund A, *et al.* Impaired regulation of the incretin effect in patients with type 2 diabetes. *J Clin Endocrinol Metab* 2011; 96: 737–745.
23. Classification and diagnosis of diabetes mellitus and other categories of glucose intolerance. National Diabetes Data Group. *Diabetes* 1979; 28: 1039–1057.
24. Alberi KG, Zimmeret PZ. Definition, diagnosis and classification of diabetes mellitus and its complications. Part 1: diagnosis and classification of diabetes mellitus provisional report of a WHO consultation. *Diabet Med* 1998; 54: 539–553.
25. Harada N, Hamasaki A, Yamane S, *et al.* Plasma GIP and GLP-1 levels after glucose loading are associated with different factors in Japanese subjects. *J Diabetes Invest* 2011; 2: 193–199.
26. Yoder SM, Yang Q, Kindel TL, *et al.* Differential responses of the incretin hormones GIP and GLP-1 to increasing doses of dietary carbohydrate but not dietary protein in lean rats. *Am J Physiol Gastrointest Liver Physiol* 2010; 299: G476–G485.
27. Brown JC, Dryburgh JR, Ross SA, *et al.* Identification and actions of gastric inhibitory polypeptide. *Recent Prog Horm Res* 1975; 31: 487–532.
28. Falko JM, Crockett SE, Cataland S, *et al.* Gastric inhibitory polypeptide (GIP) stimulated by fat ingestion in man. *J Clin Endocrinol Metab* 1975; 41: 260–265.
29. Pederson RA, Schubert HE, Brown JC. Gastric inhibitory polypeptide. Its physiologic release and insulinotropic action in the dog. *Diabetes* 1975; 24: 1050–1056.
30. Lee S, Yabe D, Nohtomi K, *et al.* Intact glucagon-like peptide-1 levels are not decreased in Japanese patients with type 2 diabetes. *Endocr J* 2010; 57: 119–126.
31. Kozawa J, Okita K, Imagawa A, *et al.* Similar incretin secretion in obese and non-obese Japanese subjects with type 2 diabetes. *Biochem Biophys Res Commun* 2010; 393: 410–413.
32. Rijkelijkhuizen JM, McQuarrie K, Girman CJ, *et al.* Effects of meal size and composition on incretin, alpha-cell, and beta-cell responses. *Metabolism* 2010; 59: 502–511.
33. Villareal DT, Robertson H, Bell GI, *et al.* TCF7L2 variant rs7903146 affects the risk of type 2 diabetes by modulating incretin action. *Diabetes* 2010; 59: 479–485.
34. Schirra J, Katschinski M, Weidmann C, *et al.* Gastric emptying and release of incretin hormones after glucose ingestion in humans. *J Clin Invest* 1996; 97: 92–103.

FEBS Letters 586 (2012) 4076–4081

FEBS Letters

journal homepage: www.FEBSLetters.org

SIRT5 deacetylates and activates urate oxidase in liver mitochondria of mice

Yasuhiko Nakamura, Masahito Ogura, Kasane Ogura, Daisuke Tanaka, Nobuya Inagaki *

Department of Diabetes and Clinical Nutrition, Graduate School of Medicine, Kyoto University, Kyoto 606-8507, Japan

ARTICLE INFO

Article history:
Received 16 August 2012
Revised 26 September 2012
Accepted 4 October 2012
Available online 16 October 2012

Edited by Vladimir Skulachev

Keywords:
SIRT5
Urate oxidase
Mouse
Liver
Mitochondria

ABSTRACT

We identified urate oxidase (UOX) as a target of SIRT5 by comparing mitochondrial proteins in livers of SIRT5-overexpressing transgenic (SIRT5 Tg) and wild-type mice by using two-dimensional electrophoresis. Acetylation levels of UOX in liver of SIRT5 Tg mice were approximately half of those in wild-type mice, and UOX activity was significantly increased. *In vitro*-synthesized UOX protein was acetylated when incubated with mitochondria from wild-type mice liver but the levels were less when incubated with those from SIRT5 Tg mice liver. These results suggest that SIRT5 activates UOX through deacetylation in mouse liver mitochondria.

Structured summary of protein interactions:
Uox physically interacts with **Sirt5** by anti bait coimmunoprecipitation (View interaction)
Catalase, **Hsp60** and **Uox** colocalize by cosedimentation through density gradient (View interaction)
Hsp60, **Uox** and **Sirt5** colocalize by cosedimentation through density gradient (View interaction)

1. Introduction

It is known that lifespan is prolonged by calorie restriction in species ranging from yeast to mice [1–3]. Recently, a 20-year longitudinal study in monkeys revealed that calorie restriction suppressed risk of development of age-associated disease involving brain atrophy, neoplasia, cardiovascular disease, and glucoregulatory impairment, thereby diminishing the incidence of age-dependent death [4]. It is also reported that disruption of SIR2, which is a NAD^+-dependent histone deacetylase in nucleus, abolishes lifespan extension by calorie restriction in yeast [5]. Mammals have seven SIR2 homologues in the SIRT family (SIRT1–7). Among them, SIRT1, SIRT2, SIRT3, and SIRT5 have NAD^+-dependent protein deacetylase activity. [6]. It is thought that SIRTs recognize the decrease in energy levels of the cell by calorie restriction as an increase in NAD^+ content [7]. SIRT5 protein, a member of the SIRT family, is known to locate in mitochondria [8–10], and has not only the NAD^+-dependent deacetylase activity but also NAD^+-dependent desuccinylase and demalonylase activities [6,11]. Recently, we [12] and the Guarente group [13] found independently that carbamoyl phosphate synthase 1 (CPS1) is a SIRT5 substrate protein by using SIRT5-overexpressing transgenic (SIRT5 Tg) mice and SIRT5 knock-out mice, respectively. CPS1 is a key enzyme in the urea cycle, which detoxifies ammonia generated in liver as a by-product of gluconeogenesis from amino acids during fasting and starvation. Ammonia is finally converted to urea in liver and is excreted from kidney. We demonstrate that SIRT5 mRNA levels are increased and that CPS1 protein is deacetylated and activated by SIRT5 during fasting in mouse liver [14]. SIRT5 also deacetylates cytochrome c [10], but its role is still unknown.

Urate oxidase (UOX) is a crucial enzyme that catalyzes conversion of urate to allantoin, which has higher water solubility than urate, the last step of purine catabolism in most mammals [14] except human and hominoid primates including chimpanzee, gorilla, and orangutan, which lack UOX activity [15]. In the present study, to clarify the novel function and physiological role of SIRT5 protein in liver of mice, we attempted to identify a novel protein that is deacetylated and regulated by SIRT5 using SIRT5 Tg mice. We demonstrate here that SIRT5 may regulate purine catabolism through deacetylation and activation of UOX protein.

2. Materials and methods

Animal experiments: The mice were housed in an air-controlled (temperature 25 °C) room with dark-light cycle (10; 14 h). Animal care and procedures were approved by the Animal Care Committee of Kyoto University. As both lines (#36, #38) of 8–12 week-old SIRT5-overexpressing transgenic (SIRT5 Tg) mice showed similar data, all experiments were performed using one line (#36) and its littermate wild-type mice [12].

Abbreviations: UOX, urate oxidase; SIRT5 Tg, SIRT5-overexpressing transgenic; CPS1, carbamoyl phosphate synthetase 1

* Corresponding author. Address: Department of Diabetes and Clinical Nutrition, Graduate School of Medicine, Kyoto University, 54 Kawahara-cho, Shogoin, Sakyo-ku, Kyoto 606 8507, Japan. Fax: +81 75 771 6601.
E-mail address: inagaki@metab.kuhp.kyoto-u.ac.jp (N. Inagaki).

0014-5793/$36.00 © 2012 Federation of European Biochemical Societies. Published by Elsevier B.V. All rights reserved.
http://dx.doi.org/10.1016/j.febslet.2012.10.009

Preparation of 10 k fraction and cytosol: Preparation of mitochondria particle-enriched 10 k fraction from liver was performed as described previously [16]. Liver from mice was disrupted in isotonic buffer (PBS containing 0.2 M mannitol, 0.07 M sucrose, and 1 mM EDTA) with potter homogenizer, followed by centrifugation at 800*g* at 4 °C for 10 min to obtain post-nuclear supernatant. Post-nuclear supernatant was centrifuged at 10,000*g* at 4 °C for 10 min to obtain the mitochondria particle-enriched precipitate and post-mitochondria supernatant. The precipitate was suspended with isotonic buffer and the 10 k fraction was obtained. Post-mitochondria supernatant was then ultracentrifuged at 100,000*g* at 4 °C for 30 min, and cytosol was obtained as a supernatant.

Separation of 10 k fraction into purified mitochondria and peroxisomes: Self-generated density gradient method with OptiPrep (COSMO BIO) was performed for separation of 10 k fractions. The fraction was suspended in 6 ml 25 % OptiPrep containing 60 mM Mops-NaOH buffer (pH7.4), 0.25 M sucrose, 1 mM EDTA, and 0.1 % (v/v) ethanol. The suspension was centrifuged at 180,000*g* at 4 °C for 3 h in a fixed-angle rotor. The fractions were collected from the density gradient by 500 μL of each upward displacement.

Two-dimensional electrophoresis and identification of protein: the 10 k fraction was lysed with rehydration buffer (8 M urea, 2% CHAPS, 50 mM DTT, 0.2% Bio-Lyte (BIO-RAD), 0.001% bromophenol blue), and applied to ReadyStrip IPG Strip (BIO-RAD) and separated by isoelectric focusing electrophoresis with a range pH 7 to pH 10 using PROTEAN IEF cell (BIO-RAD). The IPG Strip was then subjected to SDS–polyacrylamide gel electrophoresis. The obtained gel was immunoblotted using anti-acetylated lysine antibody (Cell Signaling). The acetylated proteins were visualized and analyzed using Las 4000 mini (FUJIFILM). The protein spot the intensity of which was decreased in SIRT5 Tg mice compared to wild-type mice was isolated from another two-dimensional electrophoresed gel and treated with trypsin; the peptides obtained at the indicated spot were analyzed using MALDI-TOF-MS (APRO Life Science Institute, Inc.).

Measurement of urate oxidase activity: 10 k fractions from livers of SIRT5 Tg and wild-type mice were used for determination of urate oxidase. Urate oxidase activity was assayed as described by Priest and Pitts [17]. Briefly, the reaction was started by adding the 10 k fraction to the assay mixture containing 50 mM sodium borate buffer (pH 8.5) and 0.125 mM urate sodium salt at room temperature, and the decrease in absorbance at 292 nm was measured. One unit of urate oxidase activity corresponded to degradation of 1 mmol of urate at room temperature.

Immunoprecipitation: Mitochondria lysed with PBS containing 1 % Triton X-100 were incubated with anti-acetylated lysine antibody for 16 h at 4 °C. Protein G Sepharose (GE healthcare) resin was then added and incubation was continued for 3 h. The resin was washed five times with PBS containing 0.1 % Triton X-100 and boiled with SDS sample buffer (0.2 M Tris, 10% sucrose, 10% SDS, 5 mM EDTA). The sample was analyzed by immunoblotting with anti-UOX (Cell Signaling) or anti-acetylated lysine or anti-myc (Santa Cruz) antibody.

In vitro synthesis of non-acetylated UOX and incubation with mitochondria and/or cytosol: Non-acetylated and myc-tag fused UOX protein was synthesized using PURESYSTEM classic II (BioComber). UOX-myc template DNA for PURESYSTEM classic II was synthesized by PCR using primers "GAAATTAATACGACTCACTATAGGGAGACCACAACGGTTTCCCTCTAGAAATAATTTTGTTTAACTTTAAGAAGGAGATATACCAATGGCCCATTAC", "TATTCATTACAAGTCCTCTTCAGAAATGAGCTTTTGCTCCAGCCTGGAAGGCAGCTTCC", and UOX cDNA as a template. The obtained UOX-myc template DNA was added to solution containing PURESYSTEM solution A, PURESYSTEM solution B, 2 μg/μl purified liver mitochondria from SIRT5 Tg mice or wild-type mice, and/or 2 μg/μl mice liver cytosol, and incubated for 1 h at 37 °C. Obtained solutions were lysed with 1% Triton X-100 and immunoprecipitated using anti-myc antibody and then analyzed by immunoblotting using anti-myc antibody or anti-acetylated lysine antibody.

3. Results

3.1. Identification of UOX as a target of SIRT5 protein

We already established two SIRT5-overexpressing transgenic (SIRT5 Tg) mice lines [10]. We hypothesize that deacetylation of SIRT5 substrate proteins may be promoted in liver of SIRT5 Tg mice compared to that in wild-type mice. To search for a novel substrate protein of SIRT5, we performed two-dimensional electrophoresis and immunoblotting using anti-acetylated lysine antibody. As SIRT5 is expressed in mitochondria, mitochondria-enriched 10 k fractions from livers of SIRT5 Tg and wild-type mice were prepared and subjected to isoelectric focusing electrophoresis, and separated by SDS–PAGE. The acetylated proteins were then observed by immunoblotting with anti-acetylated lysine antibody. One of the proteins with spots having decreased intensity in liver of SIRT5 Tg mice (Fig. 1A, indicated by arrows) was picked up from another electrophoresed two-dimensional gels of 10 k fraction in wild-type mice, treated with trypsin, and analyzed by MALDI-TOF-MS (Fig. 1B). The protein was identified as urate oxidase (UOX) from peptide sequences determined by mass spectrometry (Table 1).

3.2. UOX is located both in mitochondria and peroxisomes

In mice, localization of UOX is controversial; some reports demonstrate that UOX is located in mitochondria [18,19] while others find localization in peroxisomes [20]. In fact, mitochondria-enriched 10 k fraction from liver of wild-type mice contains not only mitochondria but also peroxisomes. Thus, to clarify subcellular distribution of UOX, we performed self-generated density gradient by high-speed ultracentrifugation using OptiPrep to separate mitochondria from peroxisomes.

The 10 k fraction prepared from liver of wild-type mice was suspended by 25% OptiPrep solution, and ultracentrifuged at 180,000*g* at 4 °C. Samples were collected from the obtained density gradient by 500 μL of each upward displacement, and analyzed by immunoblotting using anti-hsp60 antibody as a mitochondrial marker, anti-catalase antibody as a peroxisomes marker, anti-UOX antibody, and anti-SIRT5 antibody (Fig. 2A). Mitochondria were distributed mainly in the top fractions of the density gradient, while peroxisomes were distributed mainly in the bottom fractions. UOX was distributed in both the top and bottom fractions, suggesting that UOX is located both in mitochondria and peroxisomes. To ascertain localization of UOX, we collected the top and bottom three fractions as the purified mitochondria and peroxisomes fractions, respectively, and the purified fractions were subjected to immunoblotting for hsp60, catalase, UOX, and SIRT5 (Fig. 2B). The relative ratio of SIRT5 protein level in mitochondria and peroxisomes fractions was not significantly different from that of hsp60, suggesting that SIRT5 is localized only in mitochondria. The relative ratio of UOX protein level in purified mitochondria fraction was significantly higher than that of contaminated catalase in purified mitochondria fraction, indicating that UOX is located both in peroxisomes and mitochondria.

3.3. UOX is deacetylated and activated in liver mitochondria of SIRT5 Tg mice

To confirm the result of two-dimensional electrophoresis, 10 k fractions from SIRT5 Tg and wild-type mice were lysed by Triton-X 100 and immunoprecipitated using anti-UOX antibody. The

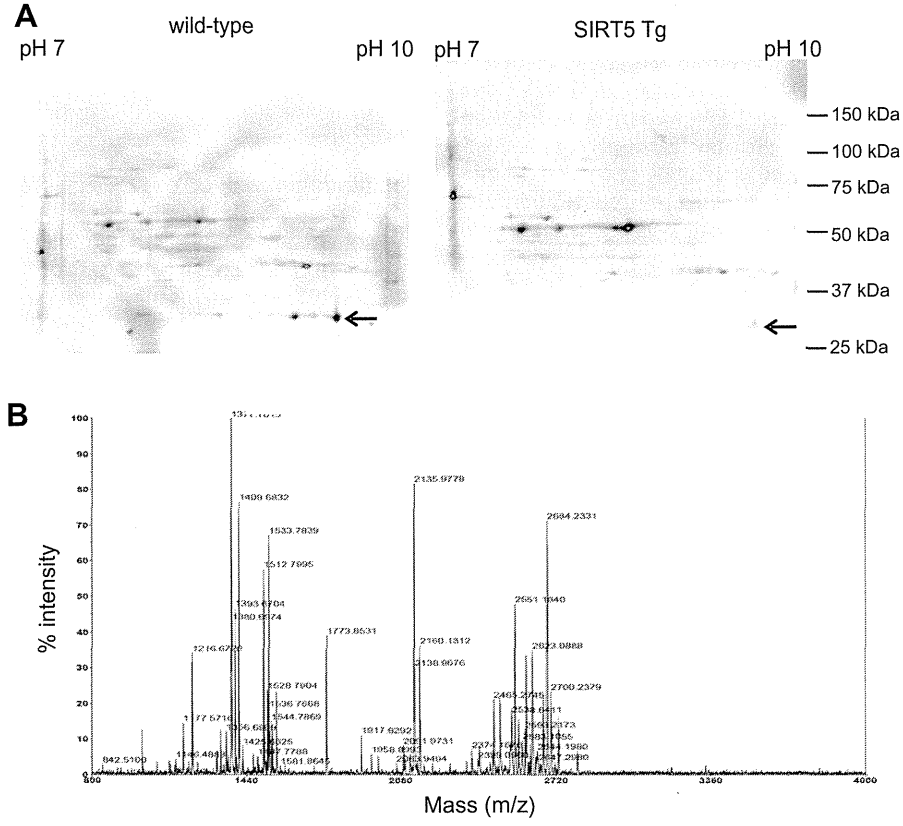

Fig. 1. Identification of the target protein of SIRT5. (A) Immunoblot analyses of two-dimensional electrophoresed gels of the mitochondria-enriched 10 k proteins prepared from livers of SIRT5 Tg and wild-type mice. The acetylated proteins were detected by immunoblotting using anti-acetylated lysine antibody. The position of the mitochondrial protein prepared from wild-type liver identified by MALDI-TOF-MS is shown by arrow (left panel). The acetylation level is decreased at the corresponding position in SIRT5 Tg liver (indicated by arrow, right panel). (B) MALDI-TOF-MS analysis. The mitochondrial protein prepared from wild-type liver indicated in (A) was analyzed using MALDI-TOF-MS.

Table 1
Characterization by MALDI-TOF-MS of the target protein of SIRT5.

Measured peptide mass (Da)	Corresponding UOX peptide sequence	Start-end
1006.4720	NDEVEFVR	11–18
1175.5104	CFATQVYCK	188–196
1215.6823	EVATSVQLTLR	42–52
1376.6725	DVDFEAIWGAVR	203–214
1511.7885	AHVYVEEVPWKR	108–119
1532.7736	RDVDFEAIWGAVR	202–214
1771.8417	FAGPYDKGEYSPSVQK	221–236
1915.9163	DYLHGDNSDIIPTDTIK	56–72
2158.1344	MGLINKEEVLLPLDNPYGK	272–290
2372.1900	TTQSGFEGFLKDQFTTLPEVK	165–185
2549.1693	HVHAFIHTPTGTHFCEVEQMR	127–147
2682.2319	NIETFAMNICEHFLSSFNHVTR	86–107

Mass of peptides corresponding to a tryptic digest of UOX. The corresponding sequence and position (number of amino acid residues) in the sequence are indicated.

obtained precipitates were then analyzed by SDS–PAGE followed by immunoblotting by anti-UOX and anti-acetylated lysine antibodies (Fig. 3A). The expression levels of UOX were not significantly different in SIRT5 Tg and wild-type mice, but the acetylation level of UOX in SIRT5 Tg mice was approximately half of that in wild-type mice (Fig. 3B). Furthermore, activity of UOX was measured using 10 k fraction from liver of SIRT5 Tg and wild-type mice. UOX activity was significantly increased 1.4-fold in SIRT5 Tg mice compared to that in wild-type mice (Fig. 3C). To investigate whether SIRT5 protein directly interacts with UOX protein, we performed co-immunoprecipitation assay (Fig. 3D); 10 k fraction prepared from liver of wild-type mice was lysed by 1% Triton X-100 and immunoprecipitated with or without anti-UOX antibody and Protein G Sepharose resin, and the resin were boiled with SDS sample buffer. The obtained samples were immunoblotted using anti-UOX antibody and anti-SIRT5 antibody. SIRT5 protein precipitate was detected with the precipitation of UOX protein. Therefore it indicates that SIRT5 protein directly interacts with UOX protein.

3.4. UOX is acetylated and deacetylated in liver mitochondria

From the results above, it is likely that UOX protein is deacetylated by SIRT5. However, it remains unclear how UOX is acetylated

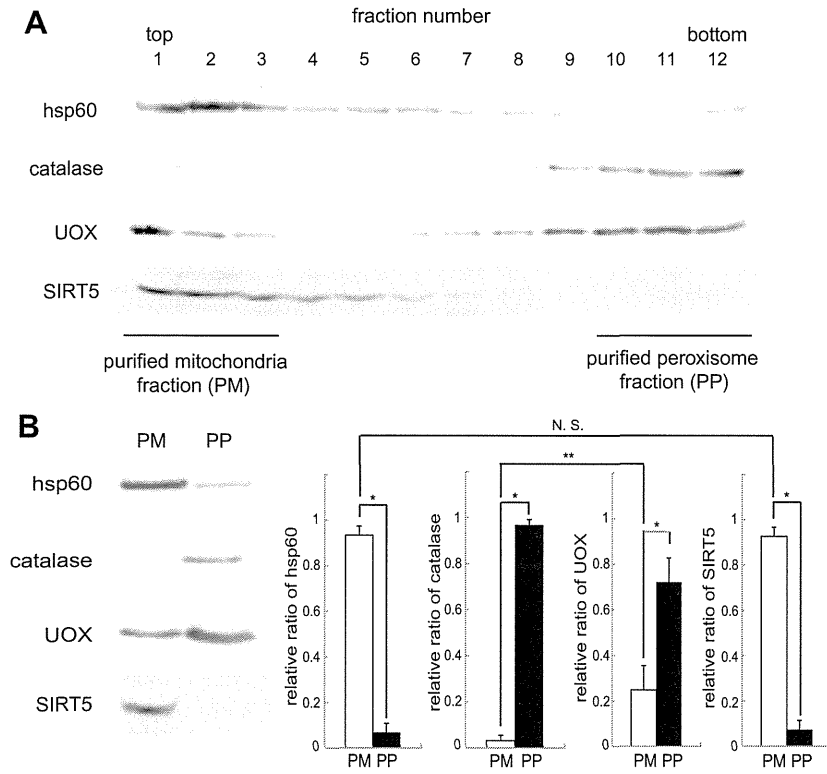

Fig. 2. Determination of UOX subcellular localization. (A) Density gradient of 10 k fraction using OptiPrep. The 10 k fraction was divided into mitochondria and peroxisomes by using self-generated density gradient. Hsp60 and catalase were used as control for mitochondria and peroxisomes, respectively. (B) UOX distribution in purified mitochondria and peroxisomes. Purified mitochondria (PM) and peroxisomes (PP) indicated in Fig. 2A were collected and immunoblotted by using anti-hsp60 (mitochondria marker), anti-catalase (peroxisomes marker), anti-UOX antibodies, and SIRT5 (left panel). Relative expression ratio of these proteins (PM/PM + PP and PP/PM + PP) are calculated by LAS-4000 mini and shown in right panel ($N = 3$). Values are means ± SEM. $^{*}P < 0.01$.$^{**}P < 0.05$. N. S.: no significant difference.

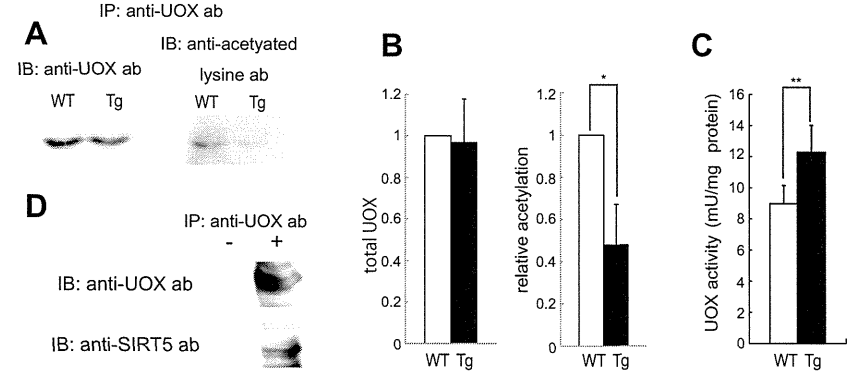

Fig. 3. Deacetylation and activation of UOX in livers of SIRT5 Tg mice. (A) UOX deacetylation in livers of SIRT5 Tg mice. The 10 k fractions from livers of SIRT5 Tg (Tg) and wild-type (WT) mice were immunoprecipitated with anti-UOX antibody, and then immunoblotted with anti-UOX antibody or anti-acetylated lysine antibody. The left two panels show immunoblotting of total UOX protein and acetylated UOX protein in mitochondria. (B) Measurement of acetylation ratio of UOX from wild-type and SIRT5 Tg mice. The ratio of acetylated UOX protein of SIRT5 Tg liver to that of wild-type liver was calculated from densitometry of immunoblotting ($N = 3$; right two panels). (C) Activation of UOX activity in SIRT5 Tg liver. 10 k fractions of livers in SIRT5 Tg ($N = 10$) and wild-type ($N = 10$) mice were used to determine the UOX activities. (D) Interaction between UOX and SIRT5. 10 k fraction was lysed by 1% Triton X-100 and immunoprecipitated with (+) or without (−) anti-UOX antibody. Then immunoblot was performed using anti-UOX antibody or anti-acetylated lysine antibody. Values are means ± SEM. $^{*}P < 0.01$. $^{**}P < 0.05$.

in the cell at physiological condition. We then investigated to find the component of the cell in which UOX protein is acetylated. First, to differentiate in vitro-synthesized UOX from endogenous UOX, UOX protein to which myc-tag was fused at C-terminus (UOX-myc) was synthesized *in vitro* (Fig. 4A). It was confirmed that there was no non-specific protein band in the UOX-myc synthetic solution by immunoblotting using anti-UOX antibody, and that the synthesized UOX protein was not acetylated by immunoblotting using anti-acetylated lysine antibody (Fig. 4A). Next, UOX-myc protein was synthesized with purified mitochondria from SIRT5 Tg mice or wild-type mice and with cytosol. After 1 h incubation, obtained suspensions were lysed by 1% Triton X-100 and immunoprecipitated by anti-myc antibody, followed by immunoblotting using anti-myc or anti-acetylated lysine antibodies (Fig. 4B). Total synthesized UOX-myc protein levels were similar in all samples. However, UOX-myc protein was acetylated only when it was incubated with mitochondria. Furthermore, acetylation levels of UOX protein in the presence of mitochondria from SIRT5 Tg mice were decreased compared to those in the presence of mitochondria from wild-type mice. These results suggest that UOX protein is acety-

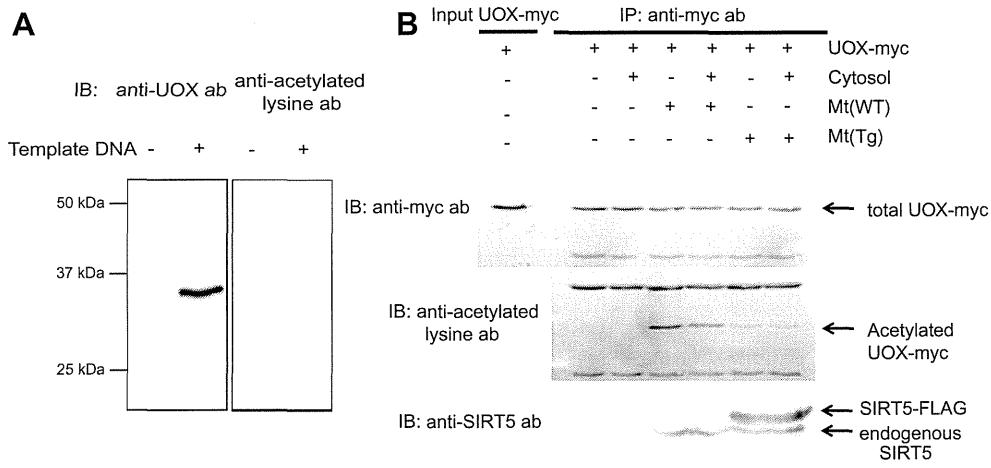

Fig. 4. Acetylation of UOX in mitochondria. (A) *In vitro* synthesis of non-acetylated UOX protein. Non-acetylated UOX-myc was synthesized by using PURESYSTEM classic II with or without UOX-myc template. Synthesized UOX-myc was validated by immunoblotteing using anti-UOX and anti-acetylated lysine antibodies. (B) Incubation of *in vitro*-synthesized UOX-myc with mitochondria. UOX-myc protein was synthesized with mice liver cytosol and/or purified mitochondria from SIRT5 Tg (Mt(Tg))mice or wilt-type (Mt(WT)) mice, and obtained solutions were lysed and immunoprecipitated using anti-myc antibody, followed by immunoblotting using anti-myc antibody (total UOC-myc) or anti-acetylated lysine antibody (acetylated UOX-myc). Mitochondrial endogenous SIRT5 and transgene derived SIRT5-FLAG are indicated in lower panel.

lated in mitochondria and that SIRT5 in mitochondria deacetylates the UOX protein.

4. Discussion

We already reported that SIRT5 mRNA expression level was significantly increased in liver of wild-type mice during fasting compared to that during feeding ad libitum [12], and Guarente group also reported SIRT5 was activated during fasting [13]. Therefore, it is thought that liver of SIRT5-overexpressing transgenic (SIRT5 Tg) mice mimics that of fasting wild-type mice.

In the present study, we attempted to identify a novel mitochondrial protein as the substrate of SIRT5 since SIRT5 is expressed in mitochondria. Mitochondria-enriched 10 k fraction from livers of SIRT5 Tg mice and littermate wild-type mice were analyzed by two-dimensional electrophoresis, immunoblotting using anti-acetylated lysine antibody, and MALDI-TOF-MS. UOX protein was identified as a novel SIRT5 substrate. There are reports showing that UOX protein locates in peroxisomes [20], but we found that UOX protein locates not only in peroxisomes but also in mitochondria using a density gradient method. In addition, our finding that *in vitro*-synthesized UOX-myc protein was acetylated when it was incubated with mitochondria strongly supports UOX localization at mitochondria. Kim et al. reported that UOX has at least 10 potential acetylation sites at lysine residues and that the acetylation state differs during ad libitum feeding and fasting in liver mitochondria [19], suggesting that lysine residue of UOX may be deacetylaed by SIRT5 during fasting.

It has been reported that SIRT5 has not only NAD^+-dependent deacetylase activity but also NAD^+-dependent desuccinylase and demalonylase activities [6,11]. Acetylation levels of UOX protein in SIRT5 Tg mice were clearly decreased compared to those in wild-type mice. However, as anti-acetylated lysine antibodies including the antibody we use here are not fully specific and also recognize differently acylated lysines, the type of UOX acyl modification removed by SIRT5 remains to be confirmed. Furthermore, we could not determine the succinylation and malonylation levels of UOX protein. Therefore, we cannot exclude the possibility that desuccinylation and demalonylation of UOX protein are involved in its activation.

In mice, knock-out of UOX gene leads to hyperuricemia and urate nephropathy and more than half of these mice die before 4 weeks of age [21]. Thus, UOX is a critical protein for survival in mice. Urate is generated in liver by purine body, which is derived mainly from skeletal muscle, and serum urate levels are elevated during fasting and starvation. In the present study, we demonstrated that acetylation levels of UOX in liver of SIRT5 Tg mice were approximately half of those in wild-type mice and that the UOX activity was significantly increased in liver of SIRT5 Tg mice compared to that in wild-type mice. Considered together, our results indicate that mRNA levels of SIRT5 are increased and that UOX protein is deacetylated and activated by SIRT5 during fasting. As we [12] and the Guarente group [13] have reported, SIRT5 regulates the urea cycle by deacetylation and activation of CPS1. SIRT5 has an important role in nitrogen metabolism at fasting and starvation state in mitochondria as both urate and urea are products of nitrogen metabolism from nucleic acid and amino acid, respectively.

To determine the cellular compartment where UOX is acetylated, we incubated in vitro-synthesized, non-acetylated UOX with mitochondria. UOX protein was not acetylated in the presence of cytosol but it was acetylated in the presence of mitochondria. In addition, UOX acetylation levels were lower when incubated with liver mitochondria of SIRT5 Tg mice in comparison with wild-type mice. These results demonstrate that the lysine residue of UOX protein is acetylated in mitochondria in physiological conditions and that there is an acetylation–deacetylation cycle in mitochondria.

In human, the UOX gene is absent. However, recombinant UOX protein is used in treatment as an anti-hyperuricemia agent in tumor lysis syndrome [22–24]. Clarifying the regulatory mechanism of UOX activation by SIRT5 should be useful to develop a more effective agent.

Acknowledgments

This study was supported by Scientific Research Grants from the Ministry of Education, Culture, Sports, Science, and Technology of Japan and from the Ministry of Health, Labor, Welfare, Japan, by a CREST grant from the Japan Science and Technology Agency, and by the Kyoto University Global COE Program "Center for Frontier Medicine".

References

[1] Imai, S., Armstrong, C.M., Kaeberlein, M. and Guarente, L. (2000) Transcriptional silencing and longevity protein Sir2 is an NAD-dependent histone deacetylase. Nature 403, 795–800.